Journal of Glaciology

Article

Cite this article: Still H, Odolinski R, Bowman MH, Hulbe C, Prior DJ (2024). Observing glacier dynamics with low-cost, multi-GNSS positioning in Victoria Land, Antarctica. *Journal of Glaciology* **70**, e31, 1–18. https://doi.org/10.1017/jog.2023.101

Received: 4 September 2023
Revised: 2 November 2023
Accepted: 13 November 2023

Keywords:
Antarctic glaciology; ice dynamics; glacier monitoring; glaciological instruments and methods

Corresponding author:
Holly Still;
Email: holly.still@postgrad.otago.ac.nz

cambridge.org/jog

Observing glacier dynamics with low-cost, multi-GNSS positioning in Victoria Land, Antarctica

Holly Still[1], Robert Odolinski[1], M. Hamish Bowman[2], Christina Hulbe[1] and David J. Prior[2]

[1]School of Surveying, University of Otago, Dunedin, New Zealand and [2]Department of Geology, University of Otago, Dunedin, New Zealand

Abstract

This study examines the performance of low-cost, low-power GNSS positioning systems for glacier monitoring in high-latitude environments. We compare the positioning performance of co-located low-cost u-blox ZED-F9P GNSS units (a few hundred USDs) and survey-grade Trimble R10 units (> $10,000 USD) under stationary (on land) and dynamic (on glacier) conditions near Terra Nova Bay, Antarctica. Low-cost and survey-grade systems yield almost identical error magnitudes under short (3 m), medium (34 km) and long (390 km) baseline kinematic-positioning scenarios. We further examined the efficacy of low-cost GNSS for glaciological applications by installing four u-blox and two Trimble receivers on Priestley Glacier to observe tide-modulated ice flexure. All receivers successfully detected subtle tidal oscillations with amplitudes < 3 cm, consistent with the predicted phasing from a tide model. These experiments offer a strong rationale for the widespread use of low-cost receivers to expand and densify GNSS monitoring networks, both in Antarctica and in glaciated regions worldwide.

1. Introduction

Ice displacement and velocity are fundamental observations used in glaciology to investigate ice mechanics and to constrain ice flow models. Measurements of ice displacement are often obtained in situ using Global Navigation Satellite Systems (GNSS), which can provide high-precision horizontal and vertical positioning and precise timing information. Applications in Antarctica include the observation of ice velocity and strain rate (Hulbe and Whillans, 1994; Minowa and others, 2019; Klein and others, 2020), observation of vertical land motion (Thomas and others, 2011; Zanutta and others, 2017; King and others, 2022), validation of satellite and radar ice altimetry data (Schröder and others, 2017; Brunt and others, 2019), and mapping of ice surface topography and surface elevation change (Hulbe and Whillans, 1997; Spikes and others, 2003; Richter and others, 2014). GNSS positioning is used to provide location and contextual information for transmitters and receivers used for geophysical surveys, including radar sounding (Horgan and others, 2017; Pratap and others, 2022), passive and active-source seismic sounding (Minowa and others, 2019; Huang and others, 2022), and gravity measurements (Zanutta and others, 2018). It is used to locate sample collection sites, including ice cores and ice-anchored moorings (Arzeno and others, 2014; Thomas and others, 2021). Many of these applications require (or could benefit from) a network of multiple GNSS devices deployed, yet this is costly and logistically challenging in polar environments.

Glaciological applications typically use geodetic or survey-grade GNSS receivers and antennas (e.g., Siegfried and others, 2016; Brunt and others, 2019; Cooley and others, 2019; Still and others, 2022). These systems are robust, reliable, and can provide dual or triple frequency, multi-GNSS data at a high rate (≥ 1 Hz), leading to centimetre-level horizontal and vertical precision under ideal conditions. However, these systems are also expensive. State-of-the-art survey-grade GNSS receiver and antenna systems can retail for ~$30,000 USD, and refurbished last-generation systems were available for ~$5,000 to $10,000 USD at the time of writing (AllTerra, 2023). High equipment costs can be prohibitive to scientific discovery, limiting the concurrent deployment of multiple GNSS receivers over large areas of interest and restricting access to users with well-financed research programmes (e.g., Chagas, 2018; Oellermann and others, 2022). Additional limitations of survey-grade receivers for deployment in remote environments include high rates of power consumption, the size and weight of receivers and antennas, and the weight of battery banks needed for multi-day installations (Willis, 2008; Jones and Rose, 2015; Jones and others, 2016).

Low-cost, mass-market GNSS chip devices—a relatively new and rapidly developing technology—are a promising alternative to the GNSS units typically used in glacier studies. These low-cost systems retail for less than 10% of the cost of survey-grade alternatives (AllTerra, 2023; U-blox, 2023). Coupled with a low-cost antenna and data logger, low-cost GNSS receivers are light and compact, with relatively low power consumption (e.g., den Ouden and others, 2010; Jones and others, 2016). The key difference between low-cost and survey-grade hardware lies in the quality of the receiver electronics. Electronic components generate internal

receiver noise that affects the continuous tracking of satellite signals and ambiguity fixing, particularly when GNSS signals are weak. Nonetheless, low-cost receivers and antennas can achieve centimetre-level precision by tracking multiple GNSS satellite constellations (e.g., GPS, GLONASS, Galileo, BeiDou, QZSS) at two or more carrier frequencies (Odolinski and Teunissen, 2016, 2020). The low-cost u-blox ZED-F9P GNSS receiver, for example, has a specified real time kinematic (RTK) positioning accuracy of 1 cm + 1 ppm CEP over a 1 km baseline in optimal conditions (U-blox, 2022a). In practice, positioning performance depends on baseline length (the distance between a reference station and moving GNSS receiver), satellite–receiver geometry, antenna and receiver hardware design, atmospheric conditions, and multipath interference errors (Odijk and Wanninger, 2017, pg. 770–773), all of which are relevant to polar applications. The performance of readily available u-blox ZED-F9P receivers is investigated here as a low-cost solution for glacier monitoring.

The precision and reliability of low-cost GNSS receivers has been evaluated for short baseline, static and dynamic positioning at mid to low latitudes (e.g., Odolinski and Teunissen, 2016; Nie and others, 2020; Xue and others, 2022). Similar performance comparisons between low-cost and survey-grade systems have not been conducted in high-latitude, glaciated environments. Of relevance to polar environments where permanent GNSS reference stations are sparse, Odolinski and Teunissen (2020) show that the positioning performance of u-blox ZED-F9P receivers is competitive with a survey-grade system in a long-baseline (112.9 km), kinematic-positioning configuration. Performance evaluations of u-blox receivers in geophysical monitoring contexts have also yielded millimetre-level precision for continuous tectonic motion (Tunini and others, 2022) and landslide detection (Notti and others, 2020; Šegina and others, 2020). In controlled, short-baseline (<100 m) RTK positioning experiments, u-blox ZED-F9P receivers paired with low-cost antennas could detect mechanically-induced horizontal displacements as small as 10 mm (Hamza and others). All of these results suggest that the measurement precision needed for glacier mechanics studies is possible with this equipment, and for this reason, u-blox GNSS hardware is evaluated in the present study.

Polar environments present challenges, limitations, and sources of error that can affect the positioning performance of both low-cost and survey-grade GNSS equipment. At high latitudes, maximum satellite elevations are lower in the sky, with no satellites passing directly overhead (King and others, 2000; Zhang and others, 2020; Di and others, 2022). This weaker satellite–receiver geometry can lead to an unfavourable vertical dilution of precision and larger vertical positioning errors (Hugentobler and Montenbruck, 2017; Alkan and others, 2022). A second source of error, multipath interference, occurs when transmitted signals are deflected off objects before reaching the receiver. Highly reflective snow and ice surfaces may amplify multipath errors, particularly when satellites are at low elevations above the horizon (e.g., Wanninger and May, 2001; Nievinski and Larson, 2014). A third source of error originates from the degradation of GNSS signals due to geomagnetic and ionospheric storms. These space weather disturbances have a greater intensity at high latitudes, near the magnetic poles (Skone and others, 2001; Doherty and others, 2003; Linty and others, 2018; Nie and others, 2022; Paziewski and others, 2022). Altogether, these error sources and the presence of low elevation satellites can affect positioning performance by decreasing the GNSS receiver signal-to-noise ratio and increasing the frequency of cycle slips, a temporary loss-of-lock on a satellite (Dabove and others, 2020; Di and others, 2022).

Performance evaluations of GNSS receivers are often undertaken in controlled, open-sky environments with favourable conditions to achieve optimal precision and accuracy. These conditions can include: a satellite–receiver geometry that minimises positioning errors, calm ionospheric conditions, short baselines (<50 km), and mitigation of low-elevation multipath errors. This study evaluates low-cost GNSS positioning performance in a high-latitude, glaciated environment in Antarctica under challenging conditions, including medium to long baselines, varying ionospheric conditions, a glacier-valley site with some loss of sky view, a highly reflective snow or ice surface, sub-zero temperatures and differing receiver and antenna models for the base station and rover. An important objective is to evaluate whether the performance of low-cost GNSS is suitable for glaciological applications that require centimetre-level precision (e.g., the detection of variability in ice velocity over timescales of hours to days).

1.1 Objectives

This study analyses the performance of low-cost, low-power GNSS positioning for glacier and ice-sheet monitoring applications in high-latitude environments. We compare the performance of u-blox ZED-F9P GNSS receivers (< $300 USD) and survey-grade Trimble R10 receivers (> $10,000 USD) under stationary (on land) and dynamic (on glacier) conditions near Terra Nova Bay, Antarctica. In each experiment, u-blox and Trimble receivers were installed alongside each other to record positions simultaneously under the same satellite geometry and environmental conditions. The u-blox receivers were paired with both low-cost patch antennas and standard surveying antennas while the Trimble R10 receivers were used with their integrated antenna.

Three experiments were performed. The first experiment compares and evaluates performance under stationary conditions on stable ground near Mario Zucchelli Station in Terra Nova Bay, Antarctica (Fig. 1). This short baseline (3 m) experiment establishes the optimal expected performance of the receivers at a high-latitude site. The second experiment compares and evaluates the performance under dynamic conditions on Priestley Glacier. Three GNSS units (2 u-blox, 1 Trimble) were installed alongside each other on an advecting ice surface. We evaluate the kinematic positioning solutions for both medium (34 km) and long baselines (390 km). The third experiment evaluates performance in a realistic glacier monitoring context: observing the tidal flexure of Priestley Glacier's left lateral shear margin. Six GNSS units (4 u-blox, 2 Trimble) were installed in across- and along-flow transects near the margin of Priestley Glacier (Fig. 1). GNSS positioning performance is evaluated in terms of precision, the repeatability or variability of a measured quantity.

Single-baseline kinematic positioning solutions are used in the present work. That is, we determine the trajectory of a moving GNSS antenna (the 'rover') relative to a single stationary base station receiver. This is a relative positioning technique and the 'baseline' is the distance between the rover and a base station. The technique requires simultaneous observations from the two receivers, one of which is installed on stationary terrain. Relative positioning eliminates satellite and receiver clock errors, and reduces errors associated with satellite orbits, ionospheric, and tropospheric delays. Centimetre-level or better precision is feasible providing that integer ambiguity resolution is achieved.

An alternative positioning method, precise point positioning (PPP), requires the deployment of only a single GNSS receiver (Zumberge and others, 1997; Kouba and Héroux, 2001). PPP is commonly used in remote polar environments where logistical difficulties or lack of access to stationary terrain are barriers to the installation of temporary base stations (King and Aoki, 2003; King, 2004). Permanent GNSS reference stations in Antarctica are sparse, distributed near coastlines, and may be

https://doi.org/10.1017/jog.2023.101 Published online by Cambridge University Press

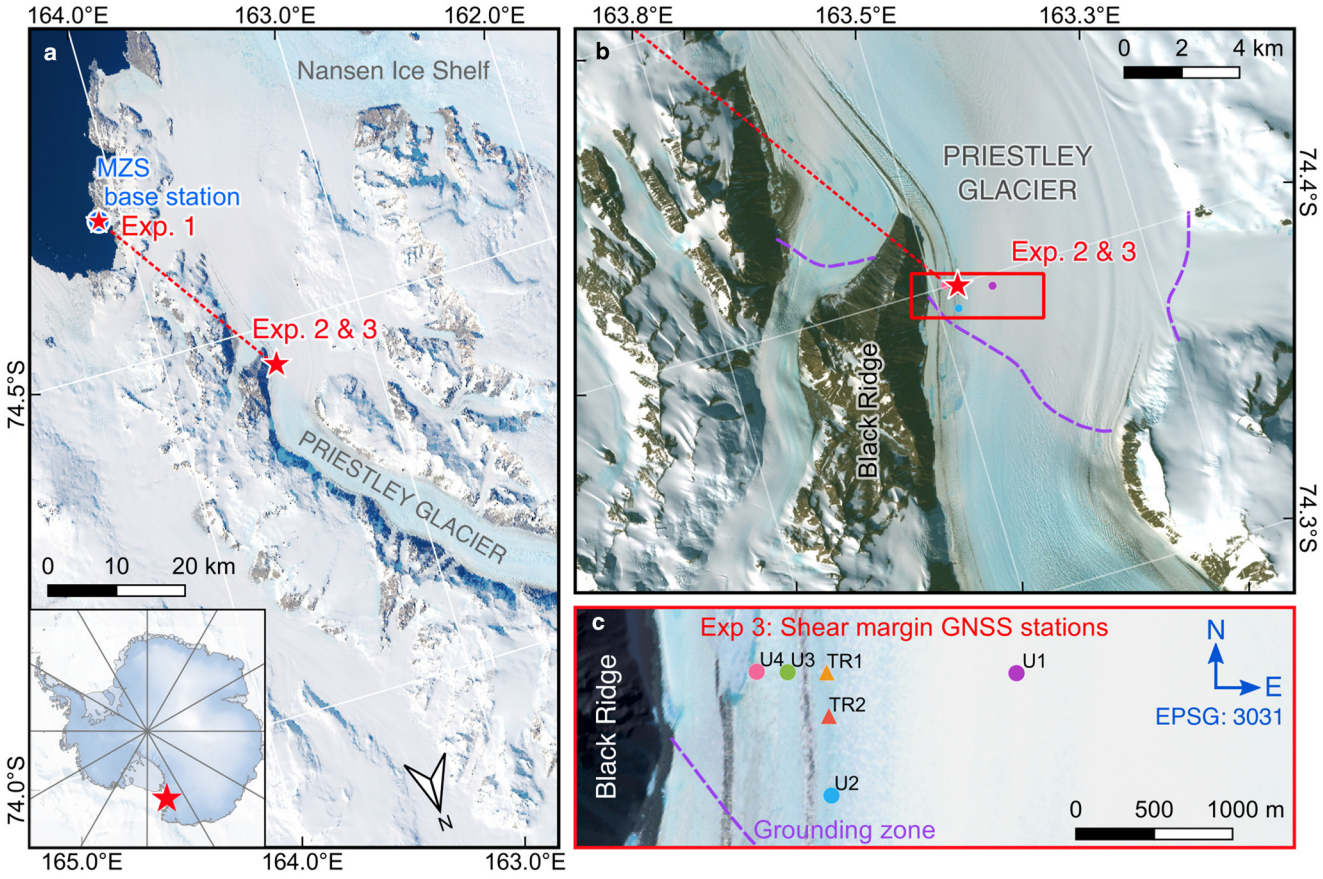

Figure 1. Site map of GNSS experiments conducted near Terra Nova Bay in the Ross Sea region, Antarctica. Map (a): the location of the stationary GNSS experiment (Experiment 1) at Mario Zucchelli Station (MZS), and the dynamic GNSS experiments on Priestley Glacier (Experiments 2 and 3). Map (b): the field site near Priestley Glacier's left lateral margin, approximately 1 km downstream from the grounding zone. Map (c): the locations of u-blox (U) and Trimble (TR) GNSS stations installed across the shear margin (Experiment 3). The estimated location of the grounding zone is from Rignot and others (2016) and the basemaps contain modified Sentinel-2, 10 m resolution imagery acquired on December 18, 2022, courtesy of the European Space Agency.

located hundreds of kilometres away from field sites. Both single-baseline kinematic positioning and PPP have produced centimetre-level precision in Antarctica, using survey-grade equipment (Hulbe and others, 2016; Schröder and others, 2017; Brunt and others, 2019; Alkan and others, 2022; Still and others, 2022). The quality of a PPP solution, however, depends on precise orbit and clock products, and the convergence time (hours rather than minutes) is significantly longer compared to relative positioning methods. If the goal is to achieve very precise 3D positions and velocities, a single-baseline kinematic positioning solution is expected to be the best-performing technique in a short to medium baseline configuration (i.e., less than 100 km between base station and rover).

2. Methods

2.1 Low-cost GNSS instrumentation

Each low-cost GNSS installation includes a receiver, antenna, data logger and power source (two 10 W, 12 V solar panels and a 12 V, 18 A h SLA battery) (Table 1). The u-blox ZED-F9P GNSS receiver module is capable of tracking GPS (L1/L2), GLONASS (L1/L2), Galileo (E1/E5b), BeiDou (B1/B2), and QZSS (L1/L2) systems and frequencies (U-blox, 2022a). The ZED-F9P module operates over a wide temperature range (−40° C to 85° C) and the rate of power consumption is relatively low (0.57 W for the u-blox ZED-F9P module + patch antenna + Arduino Cortex M0 logger, versus 1.25 W for a Trimble R10 system, and 3.67 W for a Trimble NetR9 system). The receiver is configured to log all available satellites and frequencies at 1 Hz using the software U-center v22.07 (U-blox, 2022b). RXM-RAWX messages (raw carrier phase, pseudorange, Doppler and signal quality information) and RXM-SFRBX messages (broadcast navigation data) are enabled and the raw binary u-blox files are stored with an Arduino data logger to micro SD card.

Two low-cost multiband antenna models are trialled with the u-blox receivers: the u-blox ANN-MB patch antenna (U-blox, 2022c) and an Eltehs multiband (ELT0123) standard surveying antenna (GNSS OEM, 2023) (Table 1). Patch antennas are designed to attach to flat surfaces and have magnetic bases for this purpose. We attach our patch antennas to 0.12 m diameter circular steel plates fabricated for these experiments. The plates act as a ground plane that reduces multipath interference for the otherwise exposed antennas (U-blox, 2019; Punzet and Eibert, 2023). In Experiments 1 and 2, the ground plates are bolted onto tripods. In Experiment 3, the plates are attached to uPVC glacier stakes frozen into the ice. The u-blox ANN-MB patch antenna has the advantage of a light and compact form, with the limitation of a poorer gain performance (28 dB, versus 50 dB for the Trimble R10 antenna). The gain pattern of a higher-quality antenna is optimised to suppress low elevation GNSS signals, including multipath interference (Maqsood and others, 2017).

2.2 Low-cost and survey-grade GNSS data processing

The first processing step involves a conversion from the proprietary u-blox and Trimble raw data file formats to standard

https://doi.org/10.1017/jog.2023.101 Published online by Cambridge University Press

Table 1. Specifications of the GNSS receiver and antenna hardware evaluated in each experiment. All frequency bands supported by the GNSS receivers are listed. Frequencies in bold font are used in the three experiments for a fairer comparison between u-blox and Trimble systems. Power consumption estimates are from measurements rather than manufacturer specifications. Low-cost equipment prices are from the GNSS OEM Store (https://gnss.store/) and survey-grade equipment pricing is from AllTerra (2023).

Receiver/antenna	u-blox ZED-F9P + multiband patch antenna	u-blox ZED-F9P + multiband surveying antenna	Trimble R10 (integrated antenna)
Systems and frequencies (receiver)	GPS: **L1, L2** GLO: **L1, L2** GAL: **E1, E5b** BDS: **B1, B2** QZSS: **L1, L2**	GPS: **L1, L2** GLO: **L1, L2** GAL: **E1, E5b** BDS: **B1, B2** QZSS: **L1, L2**	GPS: **L1, L2**, L5 GLO: **L1, L2**, L3 GAL: **E1, E5b**, E5a, E6 BDS: **B1, B2**, B3 QZSS: **L1, L2**, L5
Dimensions (receiver)	17.0 × 22.0 × 2.4 mm	17.0 × 22.0 × 2.4 mm	119 × 119 × 136 mm
Dimensions (antenna)	60.0 × 82.0 × 22.5 mm	160.0 × 160.0 × 66.5 mm	n/a
Weight (receiver)	< 100 g	< 100 g	1.12 kg
Weight (antenna)	173 g	400 g	n/a
Operating temp (receiver)	−40°C to +85°C	−40°C to +85°C	−40°C to +65°C
Operating temp (antenna)	−40°C to +85°C	−40°C to +70°C	n/a
Receiver price	$187 USD	$187 USD	> $10,000 USD (used)
Antenna price	$90 USD	$199 USD	n/a
Power usage of GNSS system	0.57 W	0.65 W	1.25 W
Positioning accuracy (horiz)	0.01 m +1 ppm CEP	0.01 m +1 ppm CEP	0.008 m+1 ppm RMS (RTK)
Antenna gain	28 dB	38 dB	50 dB
Experiment 1 (Fig. 2)	Rover + base station	n/a	Rover + base station
Experiment 2 (Fig. 6)	Rover (Ub2)	Rover (Ub1)	Rover (Tr1)
Experiment 3 (Fig. 1c)	Rover (Ub3, Ub4)	Rover (Ub1, Ub2)	Rover (Tr1, Tr2)

Table 2. Summary of GNSS positioning experiments conducted at Mario Zucchelli Station (MZS) and on Priestley Glacier (PG). Experiment sites are mapped in Fig. 1.

	Baseline	**Rover** receiver + antenna	**Base** receiver + antenna	Duration	Rover site	Section
Low-cost u-blox versus Trimble comparisons						
Experiment 1 (Stationary)	3.5 m	u-blox ZED-F9P + patch	u-blox F9P + patch	13 hrs	MZS	3.1
	3.5 m	Trimble R10	Trimble R10	13 hrs	MZS	
Experiment 2 (Dynamic, medium baseline)	34 km	u-blox ZED-F9P + patch	Trimble NetR9 + Zephyr	15 hrs	PG	4.1
	34 km	u-blox ZED-F9P + surveying	Trimble NetR9 + Zephyr	15 hrs	PG	
	34 km	Trimble R10	Trimble NetR9 + Zephyr	15 hrs	PG	
Experiment 2 (Dynamic, long baseline)	390 km	u-blox ZED-F9P + patch	Trimble Alloy + Zephyr 3	15 hrs	PG	4.2
	390 km	u-blox ZED-F9P + surveying	Trimble Alloy + Zephyr 3	15 hrs	PG	
	390 km	Trimble R10	Trimble Alloy + Zephyr 3	15 hrs	PG	
Application: kinematic positioning to monitor tidally-modulated ice flexure						
Experiment 3 (Dynamic)	34 km	Trimble R10	Trimble NetR9 + Zephyr	8.5 days	PG	5
	34 km	Trimble R10	Trimble NetR9 + Zephyr	7 days	PG	
	34 km	u-blox ZED-F9P + patch	Trimble NetR9 + Zephyr	4 days	PG	
	34 km	u-blox ZED-F9P + patch	Trimble NetR9 + Zephyr	4 days	PG	
	34 km	u-blox ZED-F9P + surveying	Trimble NetR9 + Zephyr	3 days	PG	
	34 km	u-blox ZED-F9P + surveying	Trimble NetR9 + Zephyr	3 days	PG	

RINEX 3.03 (Receiver Independent Exchange) files. U-blox data streams are converted using open-source RTKLIB tools (Takasu and Yasuda, 2009). Trimble observation files were converted using the Trimble 'Convert to RINEX' utility, version 3.1.4.0. GNSS stationary and dynamic observations are post-processed using the RTKPOST module within RTKLIB v2.4.3 b34 (Takasu and Yasuda, 2009; Takasu, 2013).

Multi-GNSS (GPS, GLONASS, Galileo, BeiDou and QZSS) pseudorange and carrier phase measurements are post-processed in kinematic mode using RTKLIB. A satellite elevation cut-off angle of 15° is applied to mitigate low-angle multipath or atmospheric errors. Solutions are computed at a 1 second measurement interval for short baselines (Experiment 1) to demonstrate that the low-cost system is capable of high-rate (1 Hz) data logging in this environment. For medium and long baselines (Experiments 2 and 3), solutions are computed at a 10 second measurement interval to avoid reported time correlations of several seconds in the code observations of u-blox M8T and F9P receivers (Odolinski and Teunissen, 2017a, 2020), which if neglected, may affect the positioning results. This is particularly true for medium and long baselines when relative atmospheric delays enter the model (Odolinski, 2012).

Base station and rover pairs are listed in Table 2 and kinematic processing techniques and parameters are summarised in Table 3. RTKLIB configuration settings are modified to improve the solutions for short, medium, or long baselines (e.g., Odolinski and others, 2015a). Identical processing settings are applied to each base–rover pair within each experiment and are not modified to suit a low-cost or survey-grade receiver or antenna, ensuring a fair performance comparison between the different solutions. Antenna phase centre offset (PCO) and phase centre variations (PCV) from the IGS14 antenna calibration database (IGS14.atx) are defined in RTKLIB for survey-grade Trimble observations. PCOs and PCVs are ignored for the low-cost multiband surveying antenna and ANN-MB patch antenna, although providing these values for low-cost antenna models may reduce error magnitudes by a few millimetres (Krietemeyer and others, 2022). Daily multi-GNSS broadcast ephemeris files (the BRDM00DLR* product) (Steigenberger and Montenbruck, 2020) from the CDDIS GNSS data archive (Noll, 2010) are used for short and medium baseline tests. Final multi-GNSS orbit and

https://doi.org/10.1017/jog.2023.101 Published online by Cambridge University Press

Table 3. RTKLIB configuration settings for post-processing of u-blox and Trimble position time series.

Setting	Short baseline	Medium baseline	Long baseline
Dynamic model for positions	None (kinematic)	None (kinematic)	None (kinematic)
Constellations	G, R, E, C, J	G, R, E, C, J	G, R, E
Frequencies	L1+L2	L1+L2	L1+L2
Filter type	Forward	Forward	Forward
Elevation mask	15°	15°	15°
Ionospheric modelling	Can be ignored	Estimate slant total electron content (STEC)	Estimate STEC
Wet tropospheric delay estimation	None	None	Estimate zenith tropospheric delay (ZTD) (mapping function: Niell)
Satellite ephemeris/clock	Broadcast	Broadcast	Precise
Dynamic model for ambiguities	Time constant	Time constant	Time constant

clock information (GFZ0OPSFIN* products) from the GFZ Analysis Centre (Montenbruck and others, 2017; Männel and others, 2020) are used for the long baseline (390 km) test because satellite orbit errors enter the single-baseline positioning model as the baseline increases. Output positions are provided as WGS84 latitude, longitude and ellipsoidal height. Coordinates are transformed to the Antarctic Polar Stereographic coordinate system (EPSG:3031). Time series position data are presented with the mean position for each station removed.

Smoothing or filtering techniques are often applied to processed GNSS time series to remove unrealistic peaks and high frequency noise associated with multipath interference. In Experiment 3 (Fig. 1c), in which the objective is to observe ice flexure and tidal modulation of ice velocity, outliers are removed with a three-hour moving median filter to prevent unrealistic peaks in the horizontal and vertical position time series. This method defines outliers as points that fall beyond a threshold of three scaled median absolute deviations from the sliding median. No filtering, smoothing or outlier detection methods are applied to the solutions in Experiments 1 and 2 (Section 1.1). GNSS data are presented 'as is' for the comparisons between low-cost and survey-grade receivers.

3. Experiment 1: Stationary, short-baseline positioning

This experiment quantifies the uncertainty of GNSS positions obtained with low-cost u-blox systems and directly compares the performance of u-blox and Trimble receivers under the same environmental conditions. In a short-baseline positioning configuration, ionospheric and tropospheric errors, and satellite clock and orbit errors are negligible. This stationary, short-baseline experiment therefore demonstrates the optimal expected performance of the low-cost GNSS devices for polar applications.

The stationary comparisons of low-cost u-blox and survey-grade Trimble receivers were conducted at Mario Zucchelli Station, a coastal research station located on a granite promontory in Terra Nova Bay (74.6954° S, 164.0962° E). Four GNSS units (2 low-cost u-blox ZED-F9P receivers and 2 survey-grade Trimble R10 receivers) were deployed in a base station and rover pair, on stationary ground, with a short baseline of 3.5 m (Fig. 2). Receivers and antennas were installed approximately 300 m up-slope from Mario Zucchelli Station to maximise sky view and avoid interference from buildings. Both u-blox receivers were equipped with ANN-MB patch antennas and ground plates. The Trimble R10 hardware consists of a receiver and ultra-compact Zephyr antenna within a single unit. Positions logged during the final 12 hours of the experiment, 0600 to 1800 hours (UTC) on 16 November, 2022, are analysed here. Positioning performance is evaluated in terms of the standard deviation for each component of position (east, north, up), and the 2D (horizontal) and 3D (horizontal and vertical) root mean square (RMS) errors, a collective measure of the difference between observed and expected positions. Statistics for each experiment are presented in Table 4.

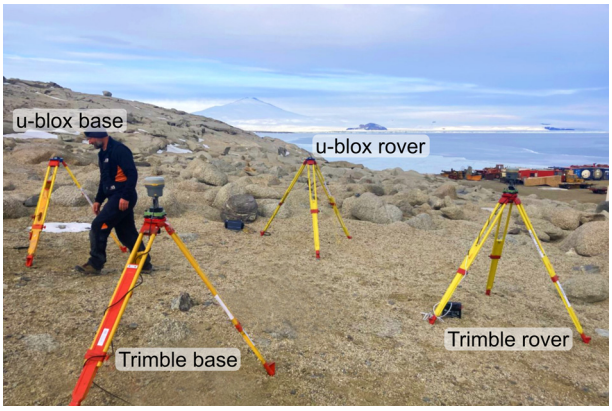

Figure 2. Low-cost u-blox and survey-grade Trimble receivers and antennas in a short-baseline (3.5 m) configuration near Mario Zucchelli Station in Terra Nova Bay, Antarctica (Experiment 1).

3.1 Short-baseline positioning performance

Satellite visibility and geometry together affect the precision of horizontal and vertical positions. Both u-blox and Trimble systems were configured to track five satellite systems visible in Antarctica (GPS, GLONASS, Galileo, BeiDou, QZSS). With an elevation cutoff angle of 15°, the u-blox system tracked a mean of 31.8 satellites (minimum = 26, maximum = 39) and the Trimble system tracked a mean of 30.0 satellites (minimum = 24, maximum = 35). The difference is due to the improved continuous signal tracking of BeiDou satellites by the u-blox receiver (Figs. 3g, h). The positional dilution of precision (PDOP) is a measure of the strength of the receiver–satellite geometry. Lower PDOP values indicate a stronger geometry (i.e., satellites are well-distributed rather than clustered across the sky). The receivers experienced similar small excursions in PDOP (Fig. 3i–j), which is reflected as an increase in noise and poorer precision, particularly in the vertical component (for example, see the epochs at 0745 UTC for the Trimble solution, column 2). Overall, excellent PDOP values approaching 1 were observed for both u-blox and Trimble systems. A PDOP >10 indicates a poor receiver–satellite geometry (e.g., Teunissen and others, 2014).

The horizontal and vertical precisions of the two systems are nearly identical (Fig. 3). The horizontal root mean square (RMS_{2D}) error is 2.4 mm for both the u-blox and Trimble GNSS stations (Table 4). The u-blox system also provided a

https://doi.org/10.1017/jog.2023.101 Published online by Cambridge University Press

Table 4. The precision of u-blox and Trimble GNSS observations. σ_e, σ_n, and σ_u denote the standard deviation of the easting, northing and vertical positions. For Experiment 2, σ_n is the standard deviation of the detrended northing positions (i.e., the mean downstream flow is removed). For Experiment 3 (dynamic observations), standard deviations σ_e, σ_n, and σ_u are computed for 30-minute moving windows and presented as the mean for each time series. The 2D (horizontal) and 3D root mean square (RMS) errors are also computed for 30-minute moving windows and presented as the mean (Experiments 2 and 3). The mean position is taken as the reference value for each RMS error calculation

	Station name	Receiver + antenna	σ_e (mm)	σ_n (mm)	σ_u (mm)	RMS_{2D} error (mm)	RMS_{3D} error (mm)
Experiment 1 (Stationary)	Ub	u-blox + patch	1.5	1.9	5.6	2.4	6.1
	Tr	Trimble R10	1.5	1.8	5.9	2.4	6.4
Experiment 2 (Dynamic, medium baseline)	Ub1	u-blox + surveying	7.0	9.6	24.4	8.4	20.2
	Ub2	u-blox + patch	8.4	9.2	26.9	9.7	23.2
	Tr1	Trimble R10	6.5	8.5	26.6	8.3	22.0
Experiment 2 (Dynamic, long baseline)	Ub1	u-blox + surveying	5.7	6.9	28.4	6.2	21.2
	Ub2	u-blox + patch	9.8	10.7	38.4	9.9	29.7
	Tr1	Trimble R10	5.3	7.5	37.4	6.5	22.4
Experiment 3 (Dynamic, medium baseline)	Ub1	u-blox + surveying	4.3	5.7	17.0	7.1	18.4
	Ub2	u-blox + surveying	4.8	6.4	15.9	8.1	17.8
	Ub3	u-blox + patch	5.1	6.7	19.4	8.7	21.1
	Ub4	u-blox + patch	5.1	6.3	18.6	8.3	20.3
	Tr1	Trimble R10	4.6	6.0	16.7	7.6	18.3
	Tr2	Trimble R10	4.0	5.5	15.0	6.9	16.5

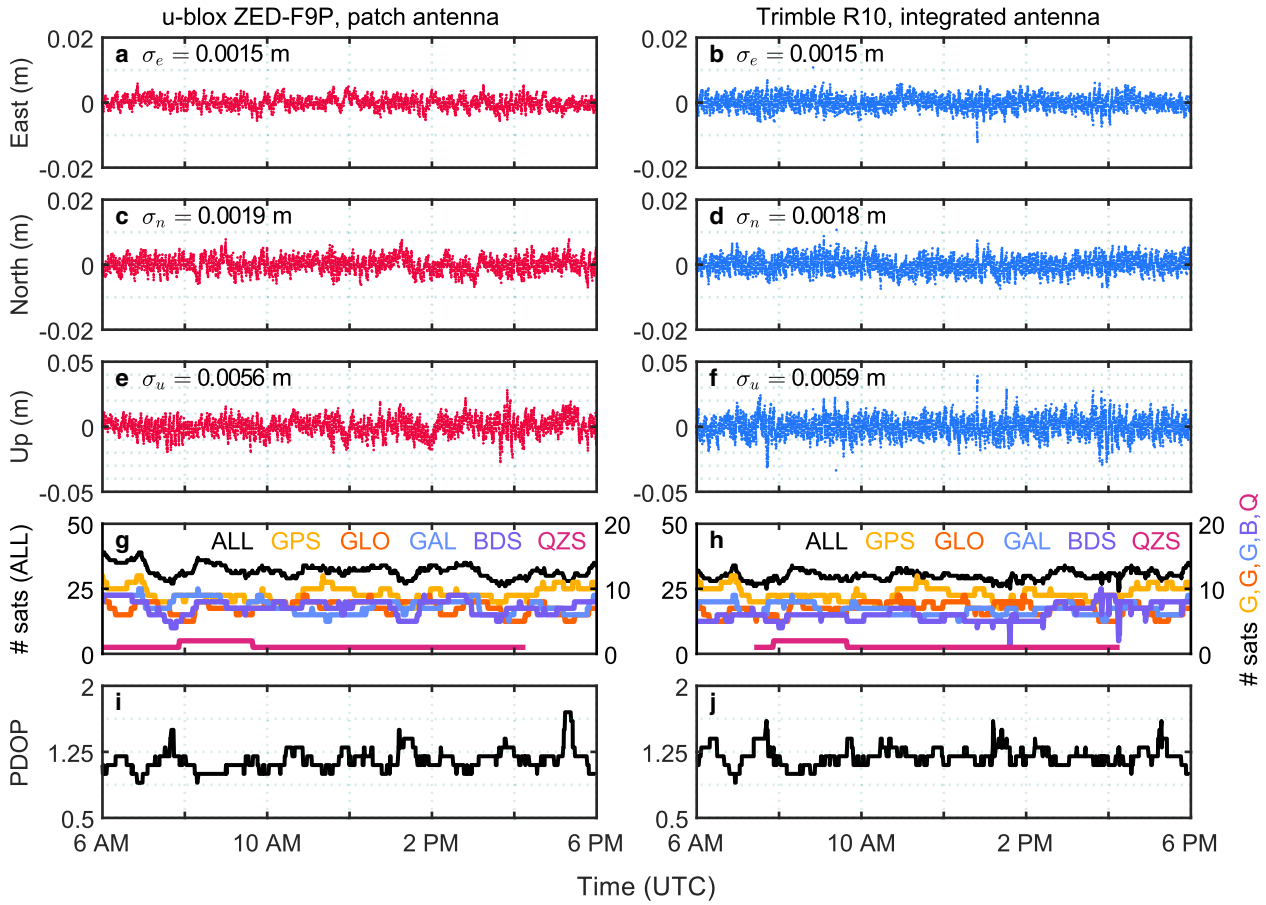

Figure 3. Short baseline, stationary positions recorded with u-blox and Trimble GNSS stations over a 12 hour observation period on 16 November, 2022 (Experiment 1). East and north components of position correspond to the horizontal axes of the Antarctic Polar Stereographic coordinate system (EPSG:3031), with the mean position removed. n = 43,200 epochs are included in each time series (1 Hz sample rate). σ is one standard deviation. The PDOP is the 3D position dilution of precision. Note the change in y-axis limits from ±2 cm for the horizontal components to ±5 cm for the vertical component.

marginal improvement in vertical precision in comparison to the Trimble system (u-blox: σ_u = 5.6 mm vs. Trimble: σ_u = 5.9 mm, Fig. 3). The corresponding 95% confidence ellipses are a 2D representation of the positional errors associated with the low-cost receiver (Fig. 4). Positioning errors are of a similar magnitude for u-blox and Trimble systems (u-blox: length of the ellipse semi-major axis = 9.4 mm vs. Trimble: 9.2 mm). The approximate north–south orientations of the ellipse semi-major axes are consistent with fewer positioning satellites traversing the southern sky at a high latitude site. This geometrical configuration, where satellite trajectories are less frequent in the southern sky, is depicted by the skyplots presented in Fig. 5.

High-precision (mm to cm-level) GNSS positions are achieved by carrier phase integer ambiguity resolution. If the number of complete carrier phase wavelengths between receiver and satellites is resolved as an integer value, the solution is fixed. Float solutions, which inherently have poorer precision, are used when integer ambiguities are not resolved. The probability of correct integer

https://doi.org/10.1017/jog.2023.101 Published online by Cambridge University Press

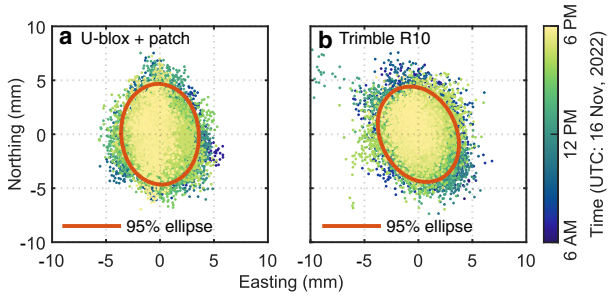

Figure 4. Horizontal positions and 2D 95% confidence ellipses for the u-blox and Trimble position time series. Confidence ellipses are computed from $n = 43{,}200$ positions obtained over 12 hours on 16 November, 2022. 'North' corresponds to grid north and the coordinate system is the same as in Fig. 3.

estimation, also referred to as the integer ambiguity success rate, is 88.6% for u-blox and 91.4% for Trimble, suggesting a similar ambiguity resolution performance between the two receivers. Solutions were classified as fixed or floating according to a commonly used ambiguity ratio test within RTKLIB with a conservative ratio threshold of three (e.g., Teunissen, 2017, pg. 680). Since the traditional ratio test is not always robust (Teunissen and Verhagen, 2009; Verhagen and Teunissen, 2013), we also evaluate positioning performance by comparing the solutions to precise benchmark coordinates. With a threshold of ±5 cm in the E/N/U directions, u-blox and Trimble systems achieved a 100.0% and 99.9% success rate, respectively, indicating a competitive performance between the two receivers. Therefore, in the following sections, we will assess the positioning performance based on solutions where ambiguities are assumed to have converged to their correct integer values. In other words, we will assess the positioning performance after convergence time for each solution.

4. Experiment 2: Dynamic, medium and long-baseline positioning

This experiment evaluates the dynamic performance of the low-cost systems in a glaciated setting. Two u-blox (Ub1 and Ub2) and one Trimble R10 (Tr1) GNSS station(s) were installed adjacent to each other on the floating left shear margin of Priestley Glacier (Fig. 6a). Station Ub1 was paired with a low-cost surveying antenna (GNSS OEM, 2023) and Ub2 was paired with a patch antenna (U-blox, 2022c) (Fig. 6b and c) to assess whether low-cost antenna type affects positioning performance. The GNSS stations were aligned in a flow-oriented transect with a 5 m spacing. Antennas were installed 2 m above the ice surface with antenna centres positioned at the same elevation to ensure equivalent sky-view conditions. Positions were logged at a 1-second measurement interval for 15 hours during the neap tide on 21 November, 2022. Maximum windspeeds of 12 knots were recorded during the experiment.

The dynamic positioning performance of the u-blox and Trimble systems is evaluated for medium (33.9 km) and long (390 km) baseline configurations. A temporary base station (Trimble NetR9 receiver + Zephyr model antenna) was installed on the roof of a shipping container GNSS laboratory at Mario Zucchelli Station to support the medium baseline (33.9 km) test. This receiver tracked GPS, GLONASS, Galileo, BeiDou and QZSS satellite signals at 1 Hz (Fig. 6e). Existing reference stations in the Terra Nova Bay region do not record all available constellations and frequencies, and thus were unsuitable for this objective (Mario Zucchelli and Jang Bogo Station reference stations: both GPS and GLONASS only). The base station used for the long baseline test is the International GNSS Service (IGS) ground station (SCTB) established near Scott Base, 390 km southeast of

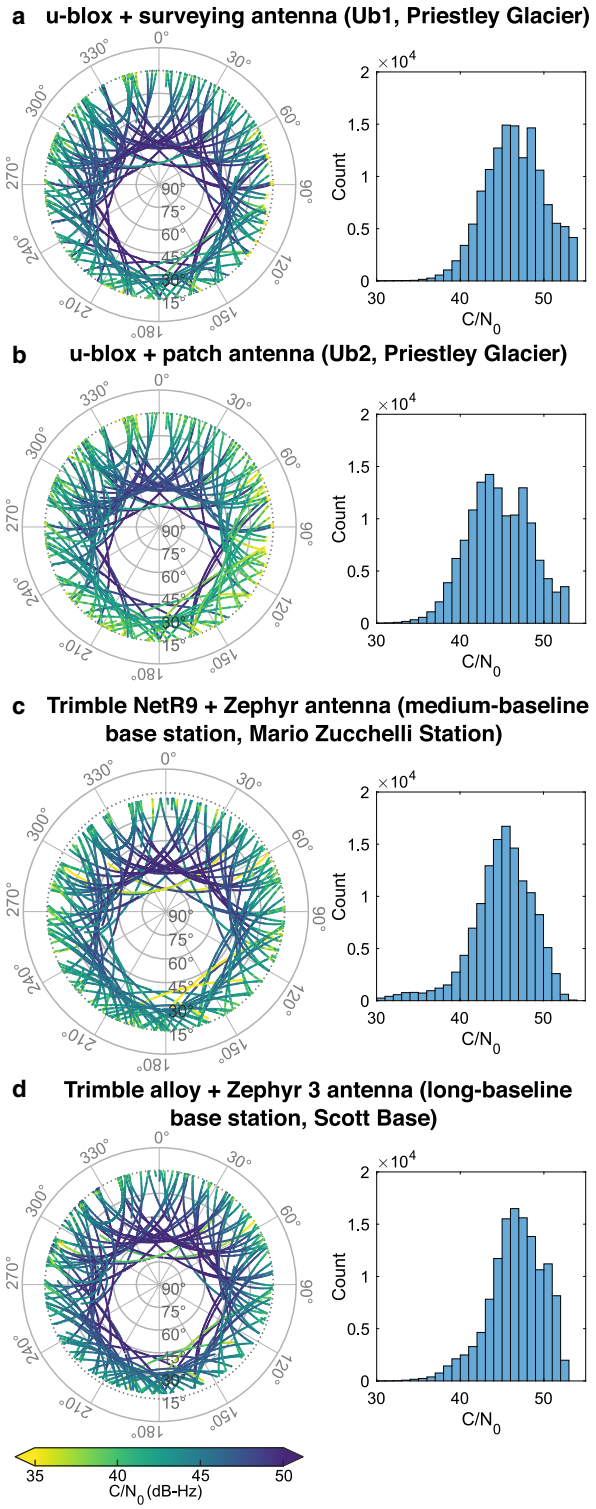

Figure 5. Satellite skyplots with carrier-to-noise (C/N_0) density ratios associated with each GNSS unit. Satellite trajectories in each skyplot are shown for 12 hours on 21 November, 2022 with an elevation cutoff of 15°. All constellations are included (GPS L1, GLONASS L1, Galileo E1, BeiDou B1, QZSS L1). The 0° azimuth corresponds to geographic north.

Priestley Glacier (Johnston and others, 2017; LINZ, 2023). This receiver tracks GPS, GLONASS, Galileo, BeiDou and QZSS satellite signals at a 1 second measurement interval.

4.1 Medium-baseline positioning performance

Low-cost stations Ub1 (surveying antenna) and Ub2 (patch antenna) provided millimetre-level precision (Fig. 7). Horizontal

https://doi.org/10.1017/jog.2023.101 Published online by Cambridge University Press

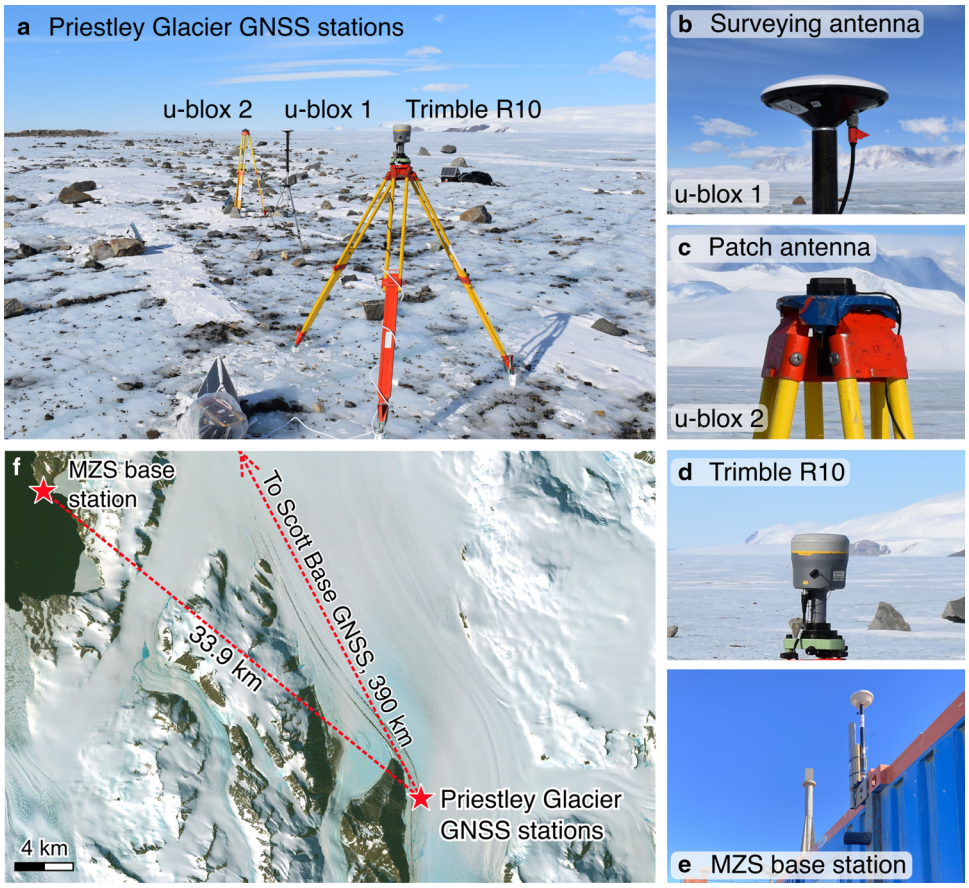

Figure 6. Low-cost u-blox and survey-grade Trimble receivers and antennas installed on Priestley Glacier for 15 hours on 21 November, 2022 (Experiment 2). Panel **(a)** demonstrates the configuration of the roving receivers. Panels **(b-d)** show the antenna models compared in the experiment. Panel **(e)** demonstrates the set-up of the temporary base station installed at Mario Zucchelli Station (MZS). Panel **(f)** illustrates the configuration of the medium (33.9 km) and long (390 km) baselines in Experiment 2. The basemap in **(f)** is a Sentinel-2, 10 m true-colour image acquired on 18 December, 2022, courtesy of the European Space Agency.

RMS_{2D} errors were 8.4 mm and 9.7 mm for Ub1 and Ub2, respectively. The u-blox receivers were competitive with the Trimble system (RMS_{2D} error: 8.3 mm), irrespective of choice of low-cost antenna (Table 4, Fig. 7). The almost identical performance of the low-cost and survey-grade instruments is also shown by similarities in the derived ice velocity estimates. Based on only 12 hours of observations, ice velocities of $99.9 \pm 0.4\ ma^{-1}$ (Ub1), $103.2 \pm 0.4\ ma^{-1}$ (Ub2), $98.9 \pm 0.3\ ma^{-1}$ (Tr1) are estimated. No tidal vertical oscillation is observed because positions were recorded during the neap tide at a site near a glacier margin.

The vertical positioning error is approximately 3 to 4 times the horizontal error for both u-blox and Trimble observations from Priestley Glacier (Table 4, Fig. 7). The ratio between the vertical and horizontal error magnitude is closer to 2 at lower latitude sites (e.g., Yong and others, 2021; Tidey and Odolinski, 2023), due to a more favourable receiver–satellite geometry. While the total number of tracked satellites at the Priestley Glacier site is relatively high (n = 30 to 32) and comparable to a mid-latitude site, the elevation angles of the satellites are lower at higher latitudes (Fig. 5). This geometry leads to a weaker vertical dilution of precision (VDOP), while the horizontal dilution of precision (HDOP) remains close to 1. A similar effect was also observed for the short baseline, stationary scenario (Experiment 1).

4.2 Long-baseline positioning performance

All GNSS stations (Ub1, Ub2, Tr1) were capable of millimetre-level horizontal precision in a long baseline (390 km) configuration (Figs. 8 and 9). Low-cost station Ub1 paired with the surveying antenna was competitive with the Trimble system (RMS horizontal errors were Ub1 = 6.2 mm and Tr1 = 6.5 mm). Of the three stations, the horizontal and vertical positions acquired with the patch antenna were more susceptible to cycle slips and measurement noise (Fig. 9). All long baseline solutions presented here use three satellite constellations only (GPS + GLONASS + Galileo). Further improvements in long-baseline positioning performance are expected with the inclusion of BeiDou and QZSS satellites (e.g., Odolinski and others, 2014; Odolinski and Teunissen, 2017b).

Vertical positioning errors for all stations increased by approximately 30% in comparison to the medium baseline errors (Table 4). Conversely, the long-baseline configuration did not increase horizontal positioning errors despite the order of magnitude increase in baseline length. With all other error sources held equal, error magnitudes increase with increasing distance between base station and rover. We attribute the better-than-expected long-baseline results to the superior antenna hardware and placement of the Scott Base IGS network station. The temporary base station installed at Mario Zucchelli Station to support the medium baseline test was located in a high-wind zone on top of a shipping container and paired with an early model, lightweight Zephyr antenna of slightly inferior quality to the IGS station antenna (Fig. 6e). The IGS station is equipped with a Zephyr 3 geodetic antenna, designed to minimise multipath via a large resistive ground plane. The difference in antenna hardware quality is shown by the distribution of the carrier-to-noise (C/N_0) density ratios (a measure of signal strength, Fig. 5), where overall,

https://doi.org/10.1017/jog.2023.101 Published online by Cambridge University Press

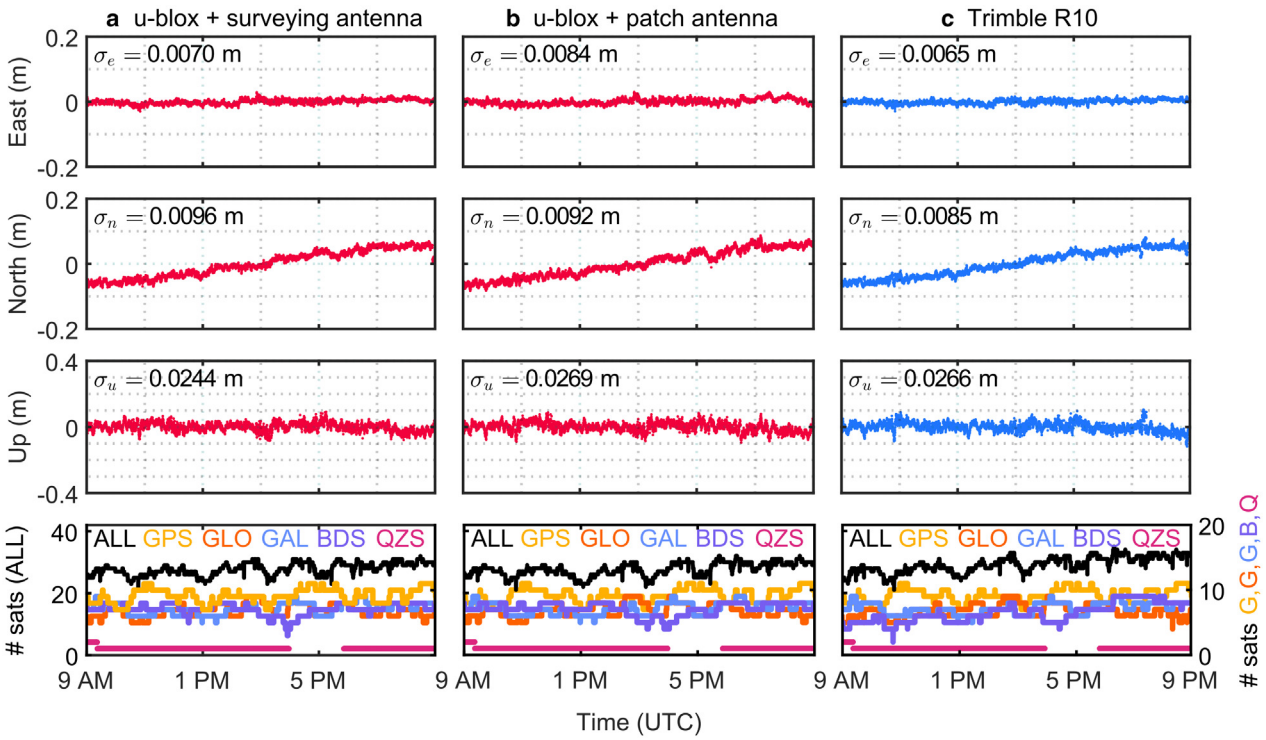

Figure 7. Medium-baseline, dynamic positions recorded with u-blox and Trimble GNSS stations installed on Priestley Glacier for a 12 hour observation period on 21 November, 2022 (Experiment 2). East and north components of position correspond to the horizontal axes of the Antarctic Polar Stereographic coordinate system (EPSG:3031), with the mean position removed. Eastings and northings also correspond to local across-flow and along-flow directions, respectively (Fig. 1c). The baseline between the NetR9 base station and the on-glacier receivers is 33.9 km. σ_e and σ_u are standard deviations and σ_n is the standard deviation of the detrended northing component of position (i.e., displacement downstream). $n = 4320$ epochs are included in each time series. Note the change in y-axis limits from ±0.2 m for the horizontal components to ±0.4 m for the vertical component.

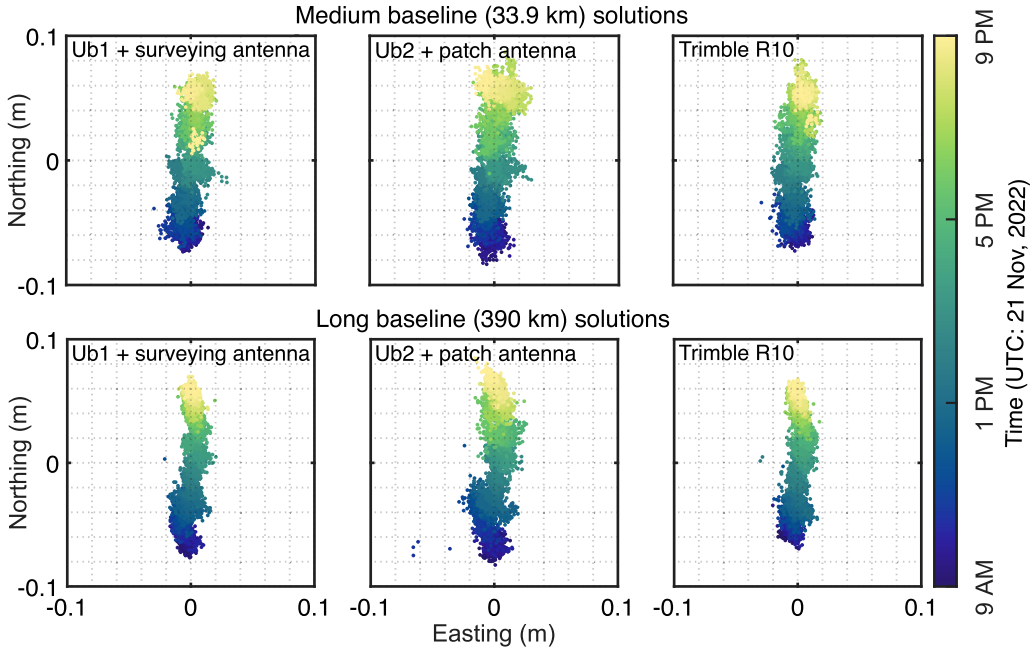

Figure 8. Horizontal trajectories of the u-blox and Trimble GNSS stations installed alongside each other on Priestley Glacier for 12 hours on 21 November, 2022 (Experiment 2). $n = 4320$ epochs are included in each solution.

observations from the Scott Base IGS station have higher C/N_0 values than the Mario Zucchelli base station.

4.3 Multi-GNSS versus GPS positioning performance

This test compares multi-GNSS solutions (GPS + GLONASS + Galileo + BeiDou + QZSS) to single (GPS) and dual-GNSS (GPS + GLONASS) solutions from the medium-baseline (33.9 km) experiment conducted on Priestley Glacier. As expected, the five-constellation positioning solution yields smaller errors than the single (GPS) and dual-GNSS (GPS + GLONASS) solutions for both u-blox and Trimble systems (Fig. 10). Each multi-GNSS positioning solution includes at least twice as many tracked satellites in comparison to the single and dual-constellation solutions,

https://doi.org/10.1017/jog.2023.101 Published online by Cambridge University Press

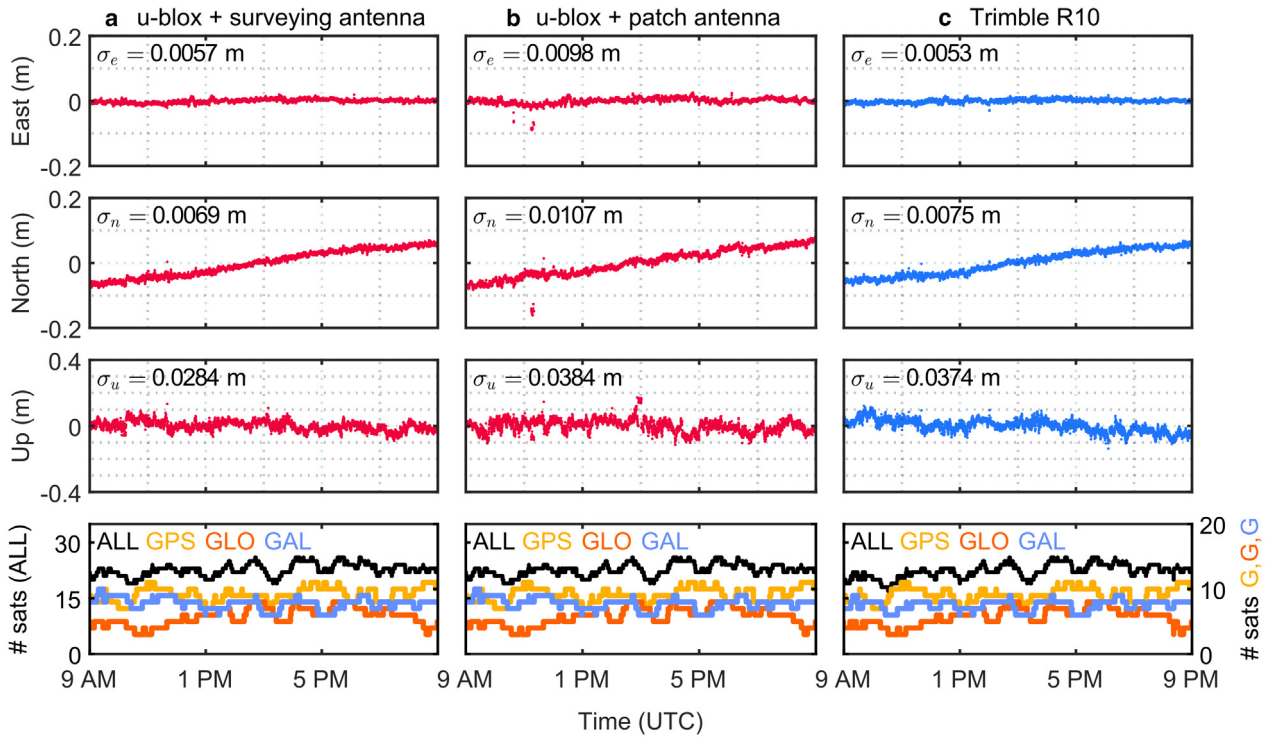

Figure 9. Long-baseline, dynamic positions recorded with u-blox and Trimble GNSS stations installed on Priestley Glacier, for a 12-hour observation period on 21 November, 2022 (Experiment 2). The baseline between the Scott Base reference station and the on-glacier receivers is 390 km. σ_e and σ_u are standard deviations and σ_n is the standard deviation of the detrended northing component of position (displacement downstream). n = 4320 epochs from a 12-hour observation period are included in each time series. Note the change in y-axis limits from ±0.2 m for the horizontal components to ±0.4 m for the vertical component.

leading to less measurement noise and a reduced frequency of undetected cycle slips that are characteristic of the single and dual-constellation solutions.

The low-cost u-blox system only achieves competitive performance to the Trimble system when three or more constellations are tracked. The Trimble system, however, provided centimetre-level precision for single (GPS) and dual (GPS + GLONASS) solutions, at epochs when the u-blox system experienced high signal noise and cycle slips (e.g,. Fig. 10, epochs at 1000 UTC). One key advantage of the higher-cost Trimble system is therefore the ability to achieve precise positions and a stable time series unaffected by cycle slips when only GPS and GLONASS observations are available. We recommend that u-blox rover and base station pairs are configured to track at least GPS, GLONASS and Galileo satellites, at two or more frequencies, for successful low-cost GNSS positioning. To summarise, the dual-GNSS system (GPS+GLONASS) provided millimetre to centimetre-level precision when using a survey-grade receiver and antenna (Fig. 10), but may not suffice when using a low-cost GNSS system at this site.

4.4 Low-cost antenna performance

The medium and long baseline experiments also evaluate the potential impact of different low-cost antenna types on the precision of the positioning results. For the long baseline, horizontal precision improved when the u-blox receiver Ub1 was paired with a multiband surveying antenna instead of a multiband patch antenna (RMS_{2D} error for Ub1: 6.2 mm vs. Ub2: 9.9 mm). Similarly, the surveying antenna also improved the vertical precision for both medium and long baseline solutions (Table 4). Antenna type had no impact on horizontal error magnitudes in the medium baseline test.

The long baseline positions obtained with a patch antenna have larger error magnitudes because the simplified antenna hardware is more susceptible to signal noise (Fig. 5). Patch antennas do not contain internal shielding to mitigate multipath effects and cycle slips are also more frequent due to the antenna receiving a weaker, noisier signal (Fig. 9b). Raw signals received by the u-blox + patch antenna system have lower C/N_0 values overall, particularly for lower elevation satellites ($< 30°$) (Figs. 5a–c). In other settings, low-cost patch antennas are also shown to have a lesser ability to suppress multipath interference and signal noise (Odolinski and Teunissen, 2017b; Romero-Andrade and others, 2021; Manzini and others, 2022; Paziewski, 2022).

5. Experiment 3: Multi-day GNSS records of ice motion

Low-cost and survey-grade GNSS performance is evaluated in a realistic glacier monitoring scenario: observing tide-modulated ice flexure across the floating shear margin of Priestley Glacier. Multi-day records of glacier motion were observed at six GNSS stations (4 u-blox, 2 Trimble R10s) arranged in across- and along-flow transects (Fig. 1c, Table 2). We present six GNSS time series of tidally-modulated across- and along-flow ice displacement and velocity with estimated positioning errors. In this experiment, the amplitudes of the E/N/U position time series for each station will vary due to the different receiver locations with respect to the glacier margin, while the timing of high and low tide peaks should be synchronised.

Vertical ice motion at a predominantly solar diurnal tidal frequency is observed at all GNSS sites (Fig. 11). Focusing on the low-cost configurations, stations Ub4 (600 m from the margin) and Ub3 (800 m from the margin), detected clear diurnal tidal oscillations with amplitudes less than 1 and 2 cm, respectively (Fig. 11a), synchronised with the timing of the CATS2008 tide

https://doi.org/10.1017/jog.2023.101 Published online by Cambridge University Press

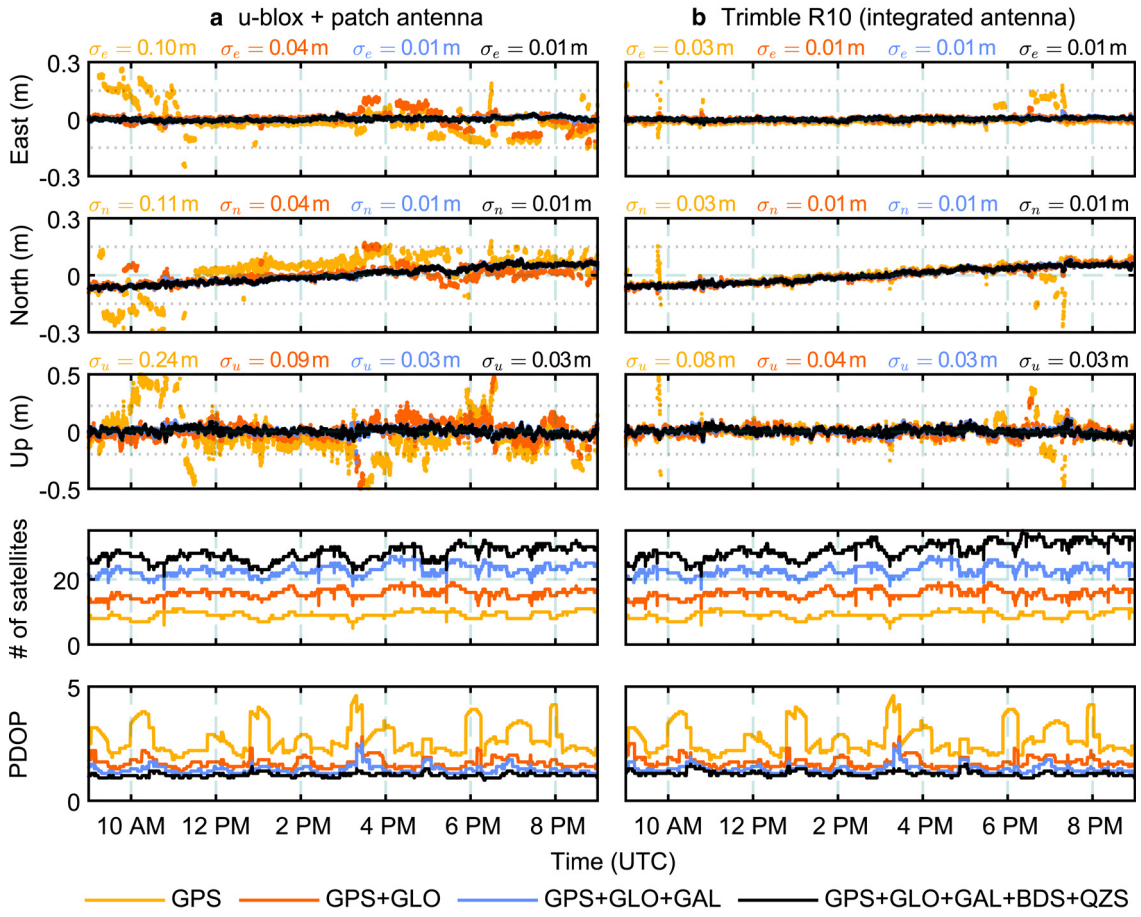

Figure 10. East (across-flow), north (along-flow) and vertical (up) positioning solutions for two Priestley Glacier GNSS stations with the inclusion of additional satellite constellations. Each time series includes $n = 4320$ epochs (10 s sample interval) collected over a 12-hour observation period on 21 November, 2022. The number of satellites is computed for an elevation cutoff angle of 15°. U-blox (a) and Trimble R10 (b) GNSS stations were installed as part of Experiment 2 (Fig. 6). Note the change in *y*-axis limits from ±0.3 m for the horizontal components to ±0.5 m for the vertical component.

prediction (Padman and others, 2002; Howard and others, 2019). Vertical positions recorded by the three GNSS stations in the along-flow transect (Fig. 11b) have very similar signal amplitudes and error magnitudes, irrespective of receiver or antenna type. Similar uncertainties are achieved in all of the GNSS configurations reported here (Fig. 11, Table 4). For example, the average of the moving standard deviation σ_u, a measure of observation noise associated with vertical positioning, is 1.9 cm (Ub3) and 1.9 cm (Ub4) for the u-blox + patch antenna configurations, and 1.7 cm (Ub1) and 1.6 cm (Ub2) when surveying antennas are used. Three explanations for the marginally smaller vertical errors derived from stations Ub1 and Ub2 are firstly the more advantageous satellite–receiver geometry – the receivers were installed a greater distance from Black Ridge and have an unobstructed skyview (Fig. 1c). Ub1 and Ub2 were also able to track an additional 1 to 2 satellites at each epoch and were paired with low-cost surveying antennas rather than patch antennas.

Tidally-modulated along- and across-flow ice displacement is observed at all GNSS stations (Fig. 12). All u-blox and Trimble stations operated with a precision that allowed the detection of velocity variability at a diurnal frequency (Fig. 12). In the along-flow direction, ice velocity increases during the falling tide, and slows during the rising tide, with one velocity maximum observed per diurnal tide cycle. In the across-flow direction, the observed transverse displacement of ice (towards and away from the margin) is associated with elastic bending. On the rising tide, ice is displaced toward the margin and on the falling tide ice is displaced toward the glacier centre (Fig. 12). The amplitude of these oscillations ranges from ±1.5 cm (Ub4, nearest the glacier margin) to ±3 cm (Ub1, nearest the glacier centre).

5.1 Sources of positioning error

In this section, we consider the causes of positioning errors at the Priestley Glacier field site. Variability in positioning noise is shown by the moving standard deviation computed for each position time series (Fig. 11b). Peaks and trends in the moving standard deviations are synchronised between all six of the GNSS stations, despite their different locations across the glacier shear margin. This consistency across GNSS stations indicates that variability in positioning noise is not predominately due to site specific multipath interference effects or differences in hardware (low-cost versus survey-grade receivers, or surveying versus patch antennas). Instead, the number of tracked satellites, or the similarities in ionospheric and tropospheric conditions, may determine the magnitude of positioning errors at the Priestley Glacier site.

Time-varying satellite geometry and atmospheric effects are demonstrated using the longest duration position time series from station Tr1 (Trimble R10, 9-day duration, Fig. 13). Short-term increases in positioning noise coincide with rapid decreases in the number of tracked positioning satellites (e.g., the epochs at 0800 hours on November 19 in Fig. 13c). The HDOP and PDOP, however, remain steady over the 9-day measurement period due the high number of positioning satellites tracked at all epochs (Fig. 13f). A second source of error, the

https://doi.org/10.1017/jog.2023.101 Published online by Cambridge University Press

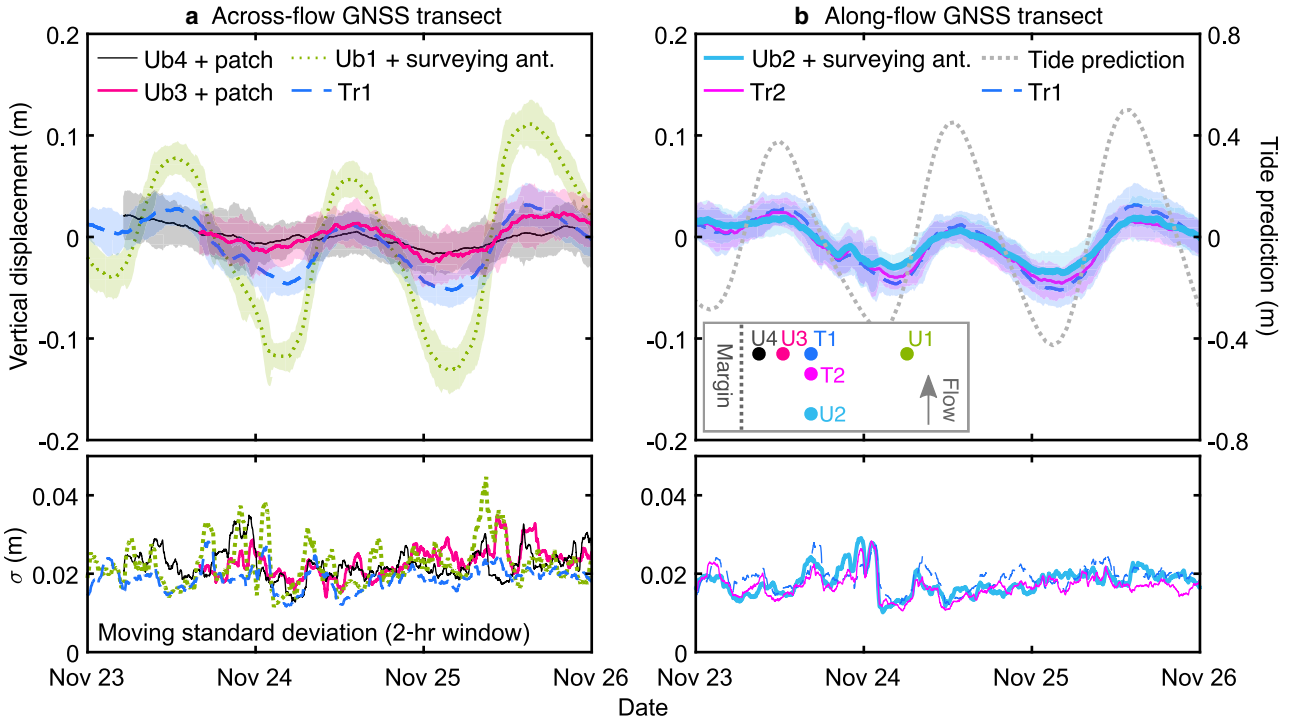

Figure 11. The tide-modulated vertical displacement of four u-blox and two Trimble GNSS stations on Priestley Glacier. Panel (a) includes the stations installed in an across-flow transect. Panel (b) includes the stations installed in an along-flow transect, and a tide prediction from the CATS2008 model (Padman and others, 2002; Howard and others, 2019). Shaded error bounds show the moving standard deviation (two-hourly window) of the vertical position time series. These GNSS stations are expected to exhibit vertical oscillations with varying amplitudes due to their different locations with respect to the glacier margin and grounding zone. Predicted tidal amplitudes and GNSS-observed amplitudes differ because the Priestley Glacier field site is not freely-floating in hydrostatic equilibrium. GNSS station locations are mapped in Fig. 1c.

prevailing ionospheric conditions (indicated by the Kp index), has no apparent association with observed positioning noise (Fig. 13e). Similarly, large variations in the slant ionospheric delay, defined as the estimated delay as the GNSS signal passes through the ionosphere, have very little association with positioning error magnitudes. This result indicates that the ionospheric delay modelling strategy (Table 3) correctly estimates the ionospheric delays. Priestley Glacier GNSS datasets were collected during a period of low to medium ionospheric disturbance (Kp index $\leq$4). A longer time series encompassing a wider range of geomagnetic disturbances is required to further investigate these effects. Indeed, low-cost GNSS hardware with poorer quality code and carrier phase measurements may be more susceptible to degraded positioning performance during periods of strong ionospheric activity.

6. Discussion

GNSS positioning performance at high latitude sites may be affected by relatively low satellite elevations, which result in weaker receiver–satellite geometries and longer signal paths through the ionosphere. Nonetheless, the positioning performance of u-blox GNSS stations at our high-latitude glacier site is similar to performance evaluations of the same equipment at mid-latitude sites. For example, kinematic positioning evaluations of u-blox receivers have reported horizontal precision of σ_e and $\sigma_n = 10$ mm (Odolinski and Teunissen, 2020) (RTK, long baseline: 112 km) and $\sigma_e = 8$ and $\sigma_n = 10$ mm (Tidey and Odolinski, 2023) (RTK, medium baseline: 27 km). In the present experiments, equivalent data processing approaches applied to low-cost and survey-grade observations with three or more constellations resulted in comparable RMS errors for each baseline length (Table 4). The high-cost, survey-grade system offered no performance advantages. At longer baselines, pairing the low-cost receiver with a ground-plane surveying antenna (rather than a patch antenna) resulted in a small improvement in precision.

The present work focuses on single-baseline kinematic positioning (a relative positioning method) because it can provide the millimetre- to centimetre-level precision required for glaciological applications. Error magnitudes are a function of baseline length, with millimetre-level precision anticipated for short baselines (< 20 km). However, the common notion that a base station must be located within a few tens of kilometres is not necessarily a requirement, particularly for dual-frequency, multi-GNSS observations. Centimetre-level precision is feasible over long baselines > 100 km (Schüler, 2006; Odolinski and Teunissen, 2020), and indeed, the present work achieved centimetre-level precision for both low-cost and survey-grade systems with a 390 km baseline (Fig. 9).

Successful positioning with the low-cost u-blox system is possible with both single-baseline kinematic positioning, and single-receiver PPP (Zumberge and others, 1997). While we use kinematic positioning due to its inherently smaller error magnitudes at short to medium baselines, remote field settings may necessitate the application of PPP techniques. To illustrate the performance of PPP with low-cost hardware, we generate example solutions using the online CSRS-PPP service (GPS+GLONASS only) and RTKLIB kinematic-PPP (GPS + GLONASS + Galileo) (see Supplementary Material). The choice of low-cost rather than survey-grade hardware did not compromise positioning performance for glaciological applications when using PPP.

6.1 Set-up of low-cost systems for successful precise positioning

The u-blox ZED-F9P receivers used here have the capability to track multi-GNSS dual-frequency signals (e.g., GPS and

https://doi.org/10.1017/jog.2023.101 Published online by Cambridge University Press

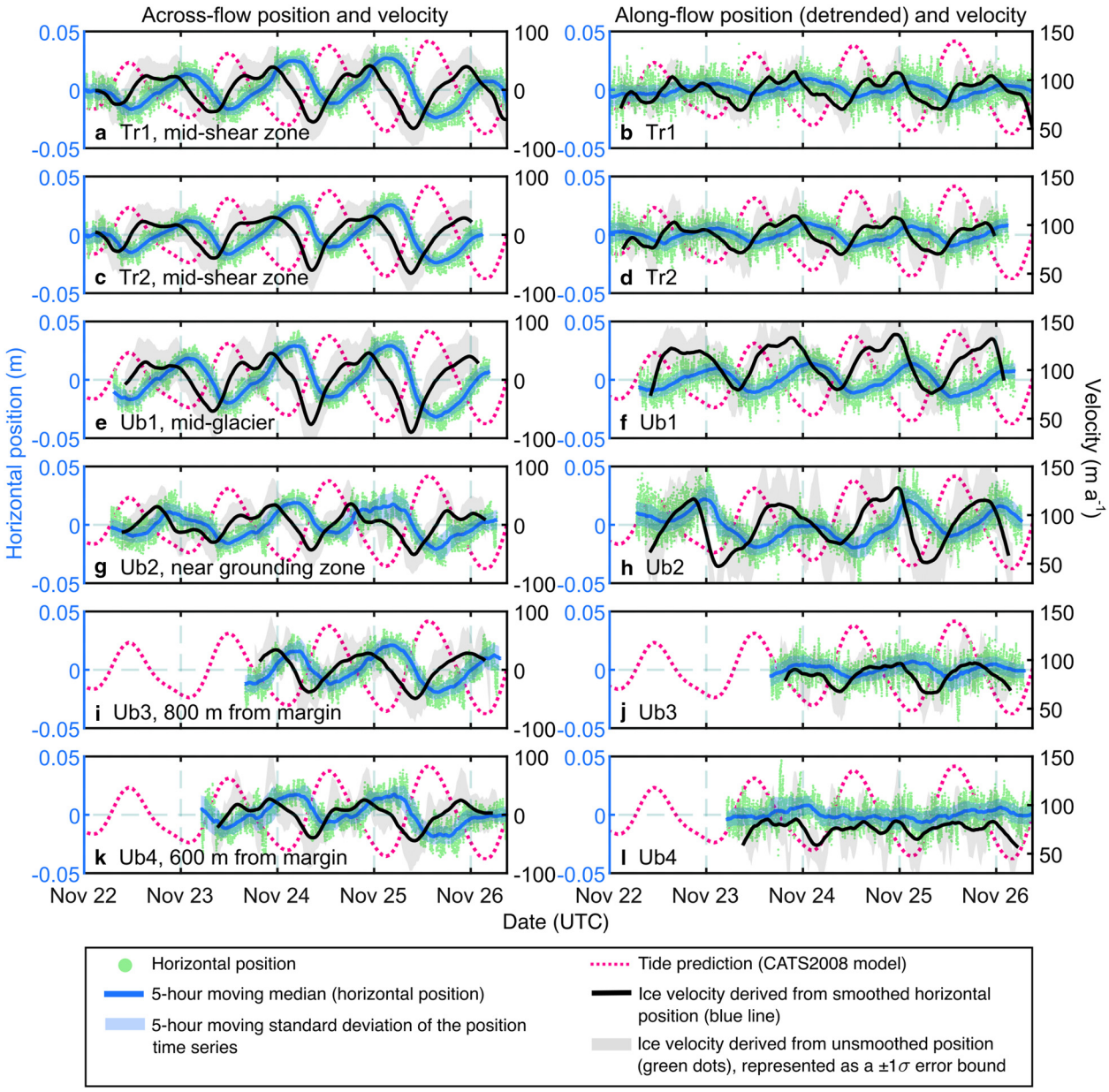

Figure 12. Across and along-flow ice displacement and velocity at each Priestley Glacier GNSS station. GNSS positions (green dots) are smoothed with a five-hour moving median filter (dark blue line). Shaded blue error bounds represent ±1σ in horizontal position over a five-hour sliding window. In column 1, across-flow displacement in the negative (positive) direction indicates motion toward (away from) the glacier margin. In column 2, the along-flow displacement is presented with the mean linear flow removed. Along-flow displacement in the positive direction indicates an increased downstream flow rate. The ice velocity (black line) is a linear least-squares fit between the smoothed displacement (blue line) and time. The grey error band denotes the velocity computed from unsmoothed positions (green dots), presented as a ±1σ error band. The tide prediction is from the CATS2008 model (Padman and others, 2002; Howard and others, 2019). Neap tide occurred on 20 November, 2022.

GLONASS: L1 and L2, Galileo: E1 and E5b). Dual-frequency observations enable medium and long-baseline positioning with low-cost systems (Odolinski and Teunissen, 2020). GNSS signals are delayed as they travel through the ionosphere, and this effect is amplified as baseline length increases and satellite elevation decreases, leading to errors on the order of tens of metres (Odijk and Wanninger, 2017). Estimation of the ionospheric delay is therefore necessary for medium and long baselines, but can be neglected for shorter baselines, in which case the delays are approximately equal. Dual-frequency data is used to estimate slant ionospheric delays, leading to more precise estimates and improved ambiguity resolution performance (Odolinski and Teunissen, 2020). In the present work, centimetre-level precision over a long baseline (390 km) is achieved in this way. Single-frequency low-cost modules will not achieve comparable results. Multi-GNSS solutions (i.e., GPS + GLONASS + Galileo + BeiDou + QZSS) provide an improved satellite geometry and redundancy in observations, leading to improvements in precision (e.g., Odolinski and others, 2015b; Paziewski and Wielgosz, 2017; Xue and others, 2021).

Single-constellation and dual-constellation solutions are widely used for GNSS positioning in Antarctica, particularly when employing PPP services such as the CSRS-PPP service (Banville and others, 2021), or when applying corrections from permanent long-term reference stations for kinematic positioning. In the latter case, existing GNSS reference stations in Antarctica are often configured to receive GPS and GLONASS signals only. For example, the nearby Mario Zucchelli and Jang Bogo Station reference GNSS stations in Terra Nova Bay both recorded GPS and GLONASS signals only during our field campaign. Installation of a temporary base station on stationary ground to track

https://doi.org/10.1017/jog.2023.101 Published online by Cambridge University Press

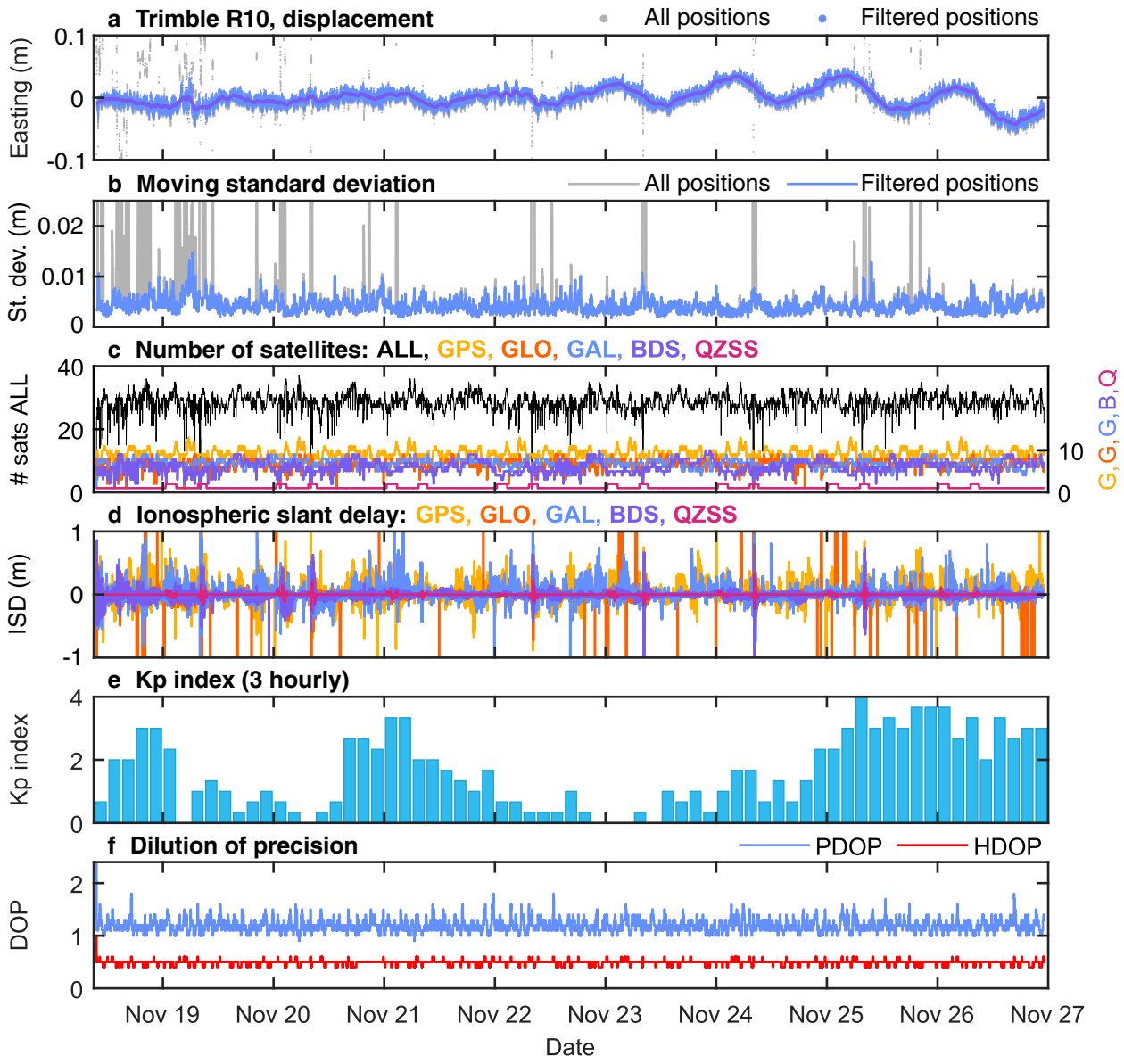

Figure 13. The association between positioning noise, satellite–receiver geometry and ionospheric conditions at station Tr1. Panel (a) shows the easting component of position. Filtered position time series have outliers removed as described in Section 2.2. Panel (b) shows the corresponding moving standard deviation, computed for 1-hourly windows (360 epochs). Panel (c) shows the number of satellites tracked at each epoch. Panels (d) and (e) show the slant ionospheric delay and the Kp index (NOAA, 2023), a measure of global ionospheric disturbance. Panel (f) shows the variability in the horizontal dilution of position (HDOP) and position 3D dilution of precision (PDOP). In this analysis, only the easting component of horizontal position is presented for brevity. Similar conclusions are drawn from time series of the northing and vertical components of position.

additional constellations may be beneficial for low-cost kinematic positioning if millimetre- to centimetre-level precision is required. The multi-GNSS solutions presented here outperformed the single or dual-constellation solutions for both low-cost and survey-grade receivers (Fig. 10).

The precision and accuracy of GNSS positions can be improved by pairing the low-cost receivers with survey-grade or geodetic antennas (e.g., Odolinski and Teunissen, 2017b; Paziewski, 2022; Romero-Andrade and others, 2021). Performance improvements associated with the use of survey-grade antennas are well established and we do not evaluate this further here. Instead, we compared the performance of low-cost patch antennas and low-cost standard surveying antennas to meet the objective of using a purely low-cost system. In cases where sub-centimetre precision is required, or when working with long baselines exceeding 100 km, using a low-cost surveying antenna rather than a patch antenna may lead to improved precision (e.g., Table 4). In the long baseline (390 km) test (Experiment 2), we observed a 30% reduction in the 3D RMS error when using a low-cost surveying antenna instead of a patch antenna.

6.2 Applications and advantages of low-cost positioning in Antarctica

The low-cost positioning systems installed on Priestley Glacier consumed approximately half as much power as the survey-grade systems (Table 2). Power usage depends on the choice of receiver, data logger, and antenna hardware (amplified surveying multi-band antenna models consume more power than patch antenna models), and the observation sampling frequency. Low-cost positioning systems used in the present work logged all available constellations at 1 Hz while supported by a pair of small 12 V solar panels (28 cm × 28 cm) and a single 18 A h SLA battery. The

https://doi.org/10.1017/jog.2023.101 Published online by Cambridge University Press

reduced power consumption of the low-cost system is a key advantage because the weight and bulkiness of an overwinter power system (battery bank + solar panels) is a burden for logistical resourcing. At present, continuous GNSS records of Antarctic ice dynamics are biased toward the summer months, with data gaps arising from the challenge of maintaining steady power supply during the polar winter (e.g., Jones and others, 2016; Greene and others, 2020; Klein and others, 2020). Low-cost GNSS stations, such as the dual-frequency u-blox units tested here, are a step toward continuous, year-round monitoring in remote environments where power requirements are logistically challenging.

Installation of a temporary low-cost base station to support a field campaign is possible without significant cost barriers. Where centimetre-level rather than decimetre-level precision is required, a low-cost, single-baseline solution may yield positions with better precision and accuracy than a PPP solution (Figs. S1 and S2). With dual-frequency receivers and multi-GNSS configurations such as the five-system (GPS + GLONASS + Galileo + BeiDou + QZSS) configuration used in the present work, medium- to long-baseline kinematic positioning (> 300 km) is feasible (Experiment 2) and may provide improved precision and accuracy over PPP (Fig. S2). Long-baseline positioning solutions can also provide redundancy and quality control when relying on PPP solutions.

The precision of the positioning system determines the smallest measurable ice displacement or change in velocity. The low-cost GNSS units tested on Priestley Glacier operated with centimetre-level horizontal and vertical precision, suitable for a range of glaciological applications. Minimum horizontal and vertical tidal oscillations detected by the low-cost systems were ~1 cm and ~1.5 cm, respectively (Figs. 11 and 12). The precision of the low-cost units is suitable for the observation of tide-modulated velocity gradients within a single week-long field campaign, with no return to the site required. Nearer to the glacier margin, where ice displacement approaches zero, measurement noise begins to exceed the amplitude of displacement, although the mean position is well defined and tide signals are still detected. Low-cost GNSS units similar to the set-ups evaluated here are also suitable for densifying existing GNSS monitoring networks or reference stations. For single-season, temporary occupations of field sites, the significantly lower cost combined with lesser power consumption motivates the deployment of additional GNSS stations for improved spatial coverage and repeatability for studies of ice kinematics and mechanics.

7. Conclusions

Low-cost, mass-market dual-frequency GNSS receivers are capable of precise and reliable positioning at high-latitude, glaciated sites, with errors comparable to high-cost systems. Horizontal and vertical positions from co-located u-blox ZED-F9P GNSS receivers (< $300 USD) and survey-grade Trimble R10 receivers (> $10,000 USD) were compared under stationary and dynamic conditions in Terra Nova Bay, Antarctica. RMS horizontal errors (Table 4) indicate almost identical performance for short baselines (u-blox + patch antenna: 2 mm, Trimble: 2 mm), medium baselines (u-blox + surveying antenna: 8 mm, Trimble: 8 mm) and long baselines (u-blox + surveying antenna: 6 mm, Trimble: 7 mm). A low-cost ground-plane surveying antenna provides a slight advantage over a patch antenna at longer baseline lengths.

Four low-cost GNSS stations and two survey-grade stations were installed on Priestley Glacier to evaluate the performance and reliability of each system in a challenging kinematic setting characterised by centimetre-level ice displacements. The efficacy of low-cost GNSS depends on the magnitude of the observation noise, relative to the signal of interest. Multi-day time series of 3D ice motion show that the low-cost systems operated with a level of precision useful for measuring tide-modulated velocity variability at semidiurnal and diurnal frequencies, at a field site where vertical ice displacement is < 5 cm per day, and horizontal ice motion is < 20 cm per day. A low-cost GNSS station installed within 600 m of the glacier margin detected tidal horizontal oscillations of ±1 cm. Such high-precision results will be reproducible in other study sites in Antarctica, providing that dual-frequency, multi-constellation receiver and antenna hardware is used.

The experiments presented here provide a 'proof of concept' of the efficacy of low-cost GNSS positioning systems for glaciological monitoring applications. The mass-market receivers and antennas evaluated here yield both a considerable cost advantage and a ~ 50% reduction in power consumption in comparison to a survey-grade system. These experiments encourage the widespread use of low-cost receivers to expand GNSS monitoring networks, both in Antarctica and in glaciated regions worldwide.

Supplementary material. The supplementary material for this article can be found at https://doi.org/10.1017/jog.2023.101

Data. The long baseline positioning uses multi-GNSS observations from the International GNSS Service (IGS) station SCTB near Scott Base, maintained by LINZ (2023) and downloaded in RINEX 3 format from the European Space Agency (ESA) GNSS Science Support Centre: https://gssc.esa.int/. Daily multi-GNSS broadcast ephemeris files (BRDM00DLR product) (Steigenberger and Montenbruck, 2020) are from the CDDIS GNSS data archive (Noll, 2010): https://cddis.nasa.gov/Data_and_Derived_Products/GNSS/gnss_mgex.html. Final multi-GNSS precise orbit and clock information (Montenbruck and others, 2017; Männel and others, 2020) generated by the GFZ Analysis Centre are available from the Analysis Center of the Multi-GNSS Experiment (MGEX): https://www.gfz-potsdam.de/en/section/space-geodetic-techniques/projects/mgex. Global Kp index values (Matzka and others, 2021) presented in Fig. 13 were downloaded from https://kp.gfz-potsdam.de/en/data. Modified Sentinel-2 images in Fig. 1 were downloaded from https://scihub.copernicus.eu/dhus/#/home.

The software u-center v22.07 is available at https://www.u-blox.com/en/product/u-center. The Trimble RINEX Converter 'ConvertToRINEX v3.14.0' software is available at https://geospatial.trimble.com/trimble-rinex-converter. Hatanaka-compressed RINEX files are uncompressed with the RNXCMP software available at: https://terras.gsi.go.jp/ja/crx2rnx.html. GNSS datasets were processed with the open-source software RTKLIB (v.2.4.3 b34, developed by T. Takasu), available at https://rtklib.com/. CSRS-PPP solutions (Banville and others, 2021) were generated with the online service: https://webapp.csrs-scrs.nrcan-rncan.gc.ca/geod/tools-outils/ppp.php. The CATS2008 tide model (Padman and others, 2002; Howard and others, 2019) used to generate the prediction in Figs. 11 and 12, is available at https://www.usap-dc.org/view/dataset/601235.

Code availability. A description of the low-cost GNSS hardware components and data logger code is available on GitHub (https://github.com/hollystill/LowCostGNSS).

Acknowledgements. HS is supported by the Antarctica New Zealand Doctoral Scholarship and the University of Otago Doctoral Scholarship. The field campaign was supported by the Marsden Fund (grant number UOO052) awarded to DJP. We express our gratitude to Antarctica New Zealand and the staff at Scott Base for logistical support. We also express our appreciation to the staff at Mario Zucchelli Station for supporting both logistical and field operations, and for assistance to install a temporary base station. We thank Brent Pooley for fabricating the ground plates used for the patch antennas, and the School of Surveying, University of Otago, for lending the Trimble GNSS equipment. The authors gratefully acknowledge T. Takasu for their contribution to developing the open-source GNSS processing software RTKLIB. We acknowledge the editor and three reviewers for their helpful feedback on the original manuscript.

Author contributions. HS and RO designed the research. MHB and HS built and configured the u-blox GNSS stations. HS, MHB and DJP collected the

GNSS datasets. HS processed the GNSS data with support from RO. HS wrote the paper with support from CH, RO, MHB and DJP.

References

Alkan RM, Erol S and Mutlu B (2022) Real-time multi-GNSS precise point positioning using IGS-RTS products in Antarctic region. *Polar Science* **32**, 100844. doi: 10.1016/J.POLAR.2022.100844

AllTerra (2023) GPS/GNSS Systems - Surveying Equipment - Products (Accessed: https://allterracentral.com/products.html/survey-equipment/gps-systems.html).

Arzeno IB and 7 others (2014) Ocean variability contributing to basal melt rate near the ice front of Ross Ice Shelf, Antarctica. *Journal of Geophysical Research: Oceans* **119**, 4214–4233. doi: 10.1002/2014JC009792

Banville S and 9 others (2021) Enabling ambiguity resolution in CSRS-PPP. *Navigation* **68**, 433–451. doi: 10.1002/NAVI.423

Brunt KM, Neumann TA and Larsen CF (2019) Assessment of altimetry using ground-based GPS data from the 88S Traverse, Antarctica, in support of ICESat-2. *Cryosphere* **13**, 579–590. doi: 10.5194/TC-13-579-2019

Chagas AM (2018) Haves and have nots must find a better way: The case for open scientific hardware. *PLOS Biology* **16**, e3000014. doi: 10.1371/JOURNAL.PBIO.3000014

Cooley J, Winberry P, Koutnik M and Conway H (2019) Tidal and spatial variability of flow speed and seismicity near the grounding zone of Beardmore Glacier, Antarctica. *Annals of Glaciology* **60**, 37–44. doi: 10.1017/aog.2019.14

Dabove P, Linty N and Dovis F (2020) Analysis of multi-constellation GNSS PPP solutions under phase scintillations at high latitudes. *Applied Geomatics* **12**, 45–52. doi: 10.1007/s12518-019-00269-4

den Ouden MAG and 5 others (2010) Stand-alone single-frequency GPS ice velocity observations on Nordenskiöldbreen, Svalbard. *Cryosphere* **4**, 593–604. doi: 10.5194/tc-4-593-2010

Di M and 7 others (2022) GNSS real-time precise point positioning in Arctic Northeast Passage. *Journal of Marine Science and Engineering* **10**, 1345. doi: 10.3390/JMSE10101345

Doherty PH, Delay SH, Valladares CE and Klobuchar JA (2003) Ionospheric scintillation effects on GPS in the equatorial and auroral regions. *Navigation* **50**, 235–245. doi: 10.1002/j.2161-4296.2003.tb00332.x

GNSS OEM (2023) GNSS RTK Multiband Antennas: L1/L2/L5 GPS, G1/G2/G3 GLONASS, B1/B2/B3 BDS, Galileo E1/E5/E6 38 dB Survey Antenna for RTK Base station. Available at: https://gnss.store/gnss-rtk-multiband-antennas/140-elt0123.html (Last accessed: August 20, 2023).

Greene CA, Gardner AS and Andrews LC (2020) Detecting seasonal ice dynamics in satellite images. *The Cryosphere* **14**, 4365–4378. doi: 10.5194/tc-14-4365-2020

Hamza V, Stopar B, Ambrožič T, Turk G and Sterle O (2020) Testing multi-frequency low-cost GNSS receivers for geodetic monitoring purposes. *Sensors* **20**, 4375. doi: 10.3390/S20164375

Horgan HJ and 6 others (2017) Poststagnation retreat of Kamb Ice Stream's grounding zone. *Geophysical Research Letters* **44**, 9815–9822. doi: 10.1002/2017GL074986

Howard SL, Padman L and Erofeeva S (2019) CATS2008: Circum-Antarctic Tidal Simulation version 2008. U.S. Antarctic Program (USAP) Data Center (Accessed: https://doi.org/10.15784/601235).

Huang MH, Lopez KU and Olsen KG (2022) Icequake-magnitude scaling relationship along a rift within the Ross Ice Shelf, Antarctica. *Geophysical Research Letters* **49**, e2022GL097961. doi: 10.1029/2022GL097961

Hugentobler U and Montenbruck O (2017) Satellite Orbits and Attitude. In Teunissen PJG and Montenbruck O (eds), *Springer Handbook of Global Navigation Satellite Systems*, 1st ed. Springer, Cham, pp. 59–90.

Hulbe CL and Whillans IM (1994) Evaluation of strain rates on Ice Stream B, Antarctica, obtained using GPS phase measurements. *Annals of Glaciology* **20**, 254–262. doi: 10.3189/1994AoG20-1-254-262

Hulbe CL and Whillans IM (1997) Weak bands within Ice Stream B, West Antarctica. *Journal of Glaciology* **43**, 377–386. doi: 10.3189/S002214300003495X

Hulbe CL and 5 others (2016) Tidal bending and strand cracks at the Kamb Ice Stream grounding line, West Antarctica. *Journal of Glaciology* **62**, 816–824. doi: 10.1017/jog.2016.74

Johnston G, Riddell A and Hausler G (2017) The International GNSS Service. In Teunissen PJG and Montenbruck O (eds), *Springer Handbook of Global Navigation Satellite Systems*, 1st ed. Springer, Cham, pp. 967–982.

Jones DH and Rose M (2015) Measurement of relative position of Halley VI modules (MORPH): GPS monitoring of building deformation in dynamic regions. *Cold Regions Science and Technology* **120**, 56–62. doi: 10.1016/j.coldregions.2015.09.010

Jones DH, Robinson C and Gudmundsson GH (2016) A new high-precision and low-power GNSS receiver for long-term installations in remote areas. *Geoscientific Instrumentation, Methods and Data Systems* **5**, 65–73. doi: 10.5194/gi-5-65-2016

King M (2004) Rigorous GPS data-processing strategies for glaciological applications. *Journal of Glaciology* **50**, 601–607. doi: 10.3189/172756504781829747

King M and Aoki S (2003) Tidal observations on floating ice using a single GPS receiver. *Geophysical Research Letters* **30**, 1138. doi: 10.1029/2002GL016182

King M, Nguyen LN, Coleman R and Morgan P (2000) Strategies for high precision processing of GPS measurements with application to the Amery Ice Shelf, East Antarctica. *GPS Solutions* **4**, 2–12. doi: 10.1007/PL00012824

King M, Watson CS and White D (2022) GPS rates of vertical bedrock motion suggest late Holocene ice-sheet readvance in a critical sector of East Antarctica. *Geophysical Research Letters* **49**, e2021GL097232, doi: 10.1029/2021GL097232

Klein E and 6 others (2020) Annual cycle in flow of Ross Ice Shelf, Antarctica: contribution of variable basal melting. *Journal of Glaciology* **66**, 861–875. doi: 10.1017/JOG.2020.61

Kouba J and Héroux P (2001) Precise point positioning using IGS orbit and clock products. *GPS Solutions* **5**, 12–28. doi: 10.1007/PL00012883

Krietemeyer A, van der Marel H, van de Giesen N and Veldhuis MCT (2022) A field calibration solution to achieve high-grade-level performance for low-cost dual-frequency GNSS receiver and antennas. *Sensors* **22**, 2267. doi: 10.3390/s22062267

Linty N, Dovis F and Alfonsi L (2018) Software-defined radio technology for GNSS scintillation analysis: bring Antarctica to the lab. *GPS Solutions* **22**, 96. doi: 10.1007/s10291-018-0761-7

LINZ (2023) PositioNZ — Toitū Te Whenua - Land Information New Zealand (Accessed: https://www.linz.govt.nz/products-services/geodetic/positionz).

Männel B and 5 others (2020) GFZ final product series for the International GNSS Service (IGS) (doi: 10.5880/GFZ.1.1.2020.002) (Accessed: https://dataservices.gfz-potsdam.de/panmetaworks/showshort.php?id=3e3bc33e-e137-11ea-9603-497c92695674).

Manzini N and 6 others (2022) Performance analysis of low-cost GNSS stations for structural health monitoring of civil engineering structures. *Structure and Infrastructure Engineering* **18**, 595–611. doi: 10.1080/15732479.2020.1849320

Maqsood M, Gao S and Montenbruck O (2017) Antennas. In Teunissen PJG and Montenbruck O (eds), *Springer Handbook of Global Navigation Satellite Systems*, 1st ed. Springer, Cham, pp. 505–534.

Matzka J, Stolle C, Yamazaki Y, Bronkalla O and Morschhauser A (2021) The Geomagnetic Kp Index and Derived Indices of Geomagnetic Activity. *Space Weather* **19**, e2020SW002641. doi: 10.1029/2020SW002641

Minowa M, Podolskiy EA and Sugiyama S (2019) Tide-modulated ice motion and seismicity of a floating glacier tongue in East Antarctica. *Annals of Glaciology* **60**, 57–67. doi: 10.1017/aog.2019.25

Montenbruck O and 12 others (2017) The multi-GNSS experiment (MGEX) of the International GNSS Service (IGS) – achievements, prospects and challenges. *Advances in Space Research* **59**, 1671–1697. doi: 10.1016/J.ASR.2017.01.011

Nie Z, Liu F and Gao Y (2020) Real-time precise point positioning with a low-cost dual-frequency GNSS device. *GPS Solutions* **24**, 9. doi: 10.1007/s10291-019-0922-3

Nie W and 6 others (2022) The mechanism for GNSS-based kinematic positioning degradation at high-latitudes under the March 2015 great storm. *Space Weather* **20**, e2022SW003132. doi: 10.1029/2022SW003132

Nievinski FG and Larson KM (2014) Inverse modeling of GPS multipath for snow depth estimation - Part I: Formulation and simulations. *IEEE Transactions on Geoscience and Remote Sensing* **52**, 6555–6563. doi: 10.1109/TGRS.2013.2297681

NOAA (2023) Geomagnetic Kp and Ap Indices (Accessed: https://www.ngdc.noaa.gov/stp/geomag/kp_ap.html).

Noll CE (2010) The crustal dynamics data information system: A resource to support scientific analysis using space geodesy. *Advances in Space Research* **45**, 1421–1440. doi: 10.1016/J.ASR.2010.01.018

https://doi.org/10.1017/jog.2023.101 Published online by Cambridge University Press

Notti D and 6 others (2020) Low-cost GNSS solution for continuous monitoring of slope instabilities applied to Madonna del Sasso Sanctuary (NW Italy). *Sensors* **20**, 289. doi: 10.3390/S20010289

Odijk D and Wanninger L (2017) Differential Positioning. In Teunissen PJG and Montenbruck O (eds), *Springer Handbook of Global Navigation Satellite Systems*, 1st ed. Springer, Cham, pp. 753–780.

Odolinski R (2012) Temporal correlation for network RTK positioning. *GPS Solutions* **16**, 147–155. doi: 10.1007/S10291-011-0213-0

Odolinski R and Teunissen PJG (2016) Single-frequency, dual-GNSS versus dual-frequency, single-GNSS: a low-cost and high-grade receivers GPS-BDS RTK analysis. *Journal of Geodesy* **90**, 1255–1278. doi: 10.1007/S00190-016-0921-X

Odolinski R and Teunissen PJG (2017a) Low-cost, high-precision, single-frequency GPS–BDS RTK positioning. *GPS Solutions* **21**, 1315–1330. doi: 10.1007/s10291-017-0613-x

Odolinski R and Teunissen PJG (2017b) Low-cost, 4-system, precise GNSS positioning: a GPS, Galileo, BDS and QZSS ionosphere-weighted RTK analysis. *Measurement Science and Technology* **28**, 125801. doi: 10.1088/1361-6501/AA92EB

Odolinski R and Teunissen PJG (2020) Best integer equivariant estimation: performance analysis using real data collected by low-cost, single- and dual-frequency, multi-GNSS receivers for short- to long-baseline RTK positioning. *Journal of Geodesy* **94**, 91. doi: 10.1007/S00190-020-01423-2

Odolinski R, Odijk D and Teunissen PJG (2014) Combined GPS and BeiDou Instantaneous RTK Positioning. *Navigation* **61**, 135–148. doi: 10.1002/NAVI.61

Odolinski R, Teunissen PJG and Odijk D (2015a) Combined GPS + BDS for short to long baseline RTK positioning. *Measurement Science and Technology* **26**, 045801. doi: 10.1088/0957-0233/26/4/045801

Odolinski R, Teunissen PJG and Odijk D (2015b) Combined BDS, Galileo, QZSS and GPS single-frequency RTK. *GPS Solutions* **19**, 151–163. doi: 10.1007/S10291-014-0376-6

Oellermann M and 6 others (2022) Open hardware in science: the benefits of open electronics. *Integrative and Comparative Biology* **62**, 1061–1075. doi: 10.1093/ICB/ICAC043

Padman L, Fricker HA, Coleman R, Howard S and Erofeeva L (2002) A new tide model for the Antarctic ice shelves and seas. *Annals of Glaciology* **34**, 247–254. doi: 10.3189/172756402781817752

Paziewski J (2022) Multi-constellation single-frequency ionospheric-free precise point positioning with low-cost receivers. *GPS Solutions* **26**, 23. doi: 10.1007/S10291-021-01209-9

Paziewski J and Wielgosz P (2017) Investigation of some selected strategies for multi-GNSS instantaneous RTK positioning. *Advances in Space Research* **59**, 12–23. doi: 10.1016/j.asr.2016.08.034

Paziewski J and 11 others (2022) The implications of ionospheric disturbances for precise GNSS positioning in Greenland. *Journal of Space Weather and Space Climate* **12**, 33. doi: 10.1051/SWSC/2022029

Pratap B and 7 others (2022) Three-decade spatial patterns in surface mass balance of the Nivlisen Ice Shelf, central Dronning Maud Land, East Antarctica. *Journal of Glaciology* **68**, 174–186. doi: 10.1017/JOG.2021.93

Punzet S and Eibert TF (2023) Impact of additional antenna groundplanes on RTK-GNSS positioning accuracy of UAVs. *Advances in Radio Science* **20**, 23–28. doi: 10.5194/ARS-20-23-2023

Richter A and 12 others (2014) Height changes over subglacial Lake Vostok, East Antarctica: Insights from GNSS observations. *Journal of Geophysical Research: Earth Surface* **119**, 2460–2480. doi: 10.1002/2014JF003228

Rignot E, Mouginot J and Scheuchl B (2016) *MEaSUREs Antarctic Grounding Line from Differential Satellite Radar Interferometry, Version 2*. NASA National Snow and Ice Data Center Distributed Active Archive Center. doi: 10.5067/IKBWW4RYHF1Q

Romero-Andrade R and 5 others (2021) Positioning evaluation of single and dual-frequency low-cost GNSS receivers signals using PPP and static relative methods in urban areas. *Applied Sciences* **11**, 10642. doi: 10.3390/APP112210642

Schröder L and 11 others (2017) Validation of satellite altimetry by kinematic GNSS in central East Antarctica. *Cryosphere* **11**, 1111–1130. doi: 10.5194/TC-11-1111-2017

Schüler T (2006) Impact of systematic errors on precise long-baseline kinematic GPS positioning. *GPS Solutions* **10**, 108–125. doi: 10.1007/S10291-005-0012-6

Šegina E and 11 others (2020) Monitoring surface displacement of a deep-seated landslide by a low-cost and near real-time GNSS system. *Remote Sensing* **12**, 3375. doi: 10.3390/RS12203375

Siegfried MR, Fricker HA, Carter SP and Tulaczyk S (2016) Episodic ice velocity fluctuations triggered by a subglacial flood in West Antarctica. *Geophysical Research Letters* **43**, 2640–2648. doi: 10.1002/2016GL067758

Skone S, Knudsen K and Jong MD (2001) Limitations in GPS receiver tracking performance under ionospheric scintillation conditions. *Physics and Chemistry of the Earth, Part A: Solid Earth and Geodesy* **26**, 613–621. doi: 10.1016/S1464-1895(01)00110-7

Spikes VB, Csathó BM and Whillans IM (2003) Laser profiling over Antarctic ice streams: Methods and accuracy. *Journal of Glaciology* **49**, 315–322. doi: 10.3189/172756503781830737

Steigenberger P and Montenbruck O (2020) In Villiger A and Dach R (eds), *Multi-GNSS Working Group Technical Report 2019*. pp. 219–229.

Still H and 10 others (2022) Tidal modulation of a lateral shear margin: Priestley Glacier, Antarctica. *Frontiers in Earth Science* **10**, 828313. doi: 10.3389/feart.2022.828313

Takasu T (2013) RTKLIB Ver. 2.4.2 Manual: RTKLIB: An Open Source Program Package for GNSS Positioning (Accessed: https://www.rtklib.com/prog/manual_2.4.2.pdf).

Takasu T and Yasuda A (2009) Development of the low-cost RTK-GPS receiver with an open source program package RTKLIB. *International symposium on GPS/GNSS*. **1**, 1–6. https://gpspp.sakura.ne.jp/paper2005/isgps_2009_rklib.pdf.

Teunissen PJG (2017) Carrier Phase Integer Ambiguity Resolution. In Teunissen PJG and Montenbruck O (eds), *Springer Handbook of Global Navigation Satellite Systems*, 1st ed. Springer, Cham, pp. 661–685.

Teunissen PJG and Verhagen S (2009) The GNSS ambiguity ratio-test revisited: A better way of using it. *Survey Review* **41**, 138–151. doi: 10.1179/003962609X390058

Teunissen PJG, Odolinski R and Odijk D (2014) Instantaneous BeiDou+GPS RTK positioning with high cut-off elevation angles. *Journal of Geodesy* **88**, 335–350. doi: 10.1007/s00190-013-0686-4

Thomas ID and 11 others (2011) Widespread low rates of Antarctic glacial isostatic adjustment revealed by GPS observations. *Geophysical Research Letters* **38**, L22302. doi: 10.1029/2011GL049277

Thomas RE and 11 others (2021) Microstructure and Crystallographic Preferred Orientations of an Azimuthally Oriented Ice Core from a Lateral Shear Margin: Priestley Glacier, Antarctica. *Frontiers in Earth Science* **9**, 702213. doi: 10.3389/feart.2021.702213

Tidey E and Odolinski R (2023) Low-cost multi-GNSS, single-frequency RTK averaging for marine applications: accurate stationary positioning and vertical tide measurements. *Marine Geodesy* **46**, 333–358. doi: 10.1080/01490419.2023.2208289

Tunini L, Zuliani D and Magrin A (2022) Applicability of cost-effective GNSS sensors for crustal deformation studies. *Sensors* **22**, 350. doi: 10.3390/S22010350

U-blox (2019) GNSS antennas: RF design considerations for u-blox GNSS receivers. Available at: https://content.u-blox.com/sites/default/files/products/documents/GNSS-Antennas_AppNote_%28UBX-15030289%29.pdf (Last accessed: 1 June, 2023).

U-blox (2022a) ZED-F9P-04B u-blox F9 high precision GNSS module. Available at: https://content.u-blox.com/sites/default/files/ZED-F9P-04B_DataSheet_UBX-21044850.pdf (Last accessed: 1 June, 2023).

U-blox (2022b) U-center GNSS evaluation software for Windows. Available at: https://content.u-blox.com/sites/default/files/u-center_Userguide_UBX-13005250.pdf (Last accessed: 1 June, 2023).

U-blox (2022c) ANN-MB series multi-band, high precision GNSS antennas. Available at: https://content.u-blox.com/sites/default/files/documents/ANN-MB_DataSheet_UBX-18049862.pdf (Last accessed: 1 June, 2023).

U-blox (2023) ZED-F9P module — u-blox. Available at: https://www.u-blox.com/en/product/zed-f9p-module (Last accessed: 1 June, 2023).

Verhagen S and Teunissen PJG (2013) The ratio test for future GNSS ambiguity resolution. *GPS Solutions* **17**, 535–548. doi: 10.1007/s10291-012-0299-z

Wanninger L and May M (2001) Carrier-phase multipath calibration of GPS reference stations. *Navigation* **48**, 112–124. doi: 10.1002/j.2161-4296.2001.tb00233.x

Willis MJ (2008) Technologies to Operate Year-Round Remote Global Navigation Satellite System (GNSS) Stations in Extreme Environments. In

Capra A and Dietrich R (eds), *Geodetic and Geophysical Observations in Antarctica*, 1st ed. Springer, Berlin, Heidelberg, pp. 11–35.

Xue C, Psimoulis P, Zhang Q and Meng X (2021) Analysis of the performance of closely spaced low-cost multi-GNSS receivers. *Applied Geomatics* **13**, 415–435. doi: 10.1007/S12518-021-00361-8

Xue C, Psimoulis PA and Meng X (2022) Feasibility analysis of the performance of low-cost GNSS receivers in monitoring dynamic motion. *Measurement* **202**, 111819. doi: 10.1016/J.MEASUREMENT.2022.111819

Yong C and 6 others (2021) Instantaneous, dual-frequency, multi-GNSS precise RTK positioning using Google Pixel 4 and Samsung Galaxy S20 smartphones for zero and short baselines. *Sensors* **21**, 8318. doi: 10.3390/S21248318

Zanutta A and 9 others (2017) Monitoring geodynamic activity in the Victoria Land, East Antarctica: Evidence from GNSS measurements. *Journal of Geodynamics* **110**, 31–42. doi: 10.1016/J.JOG.2017.07.008

Zanutta A and 9 others (2018) New geodetic and gravimetric maps to infer geodynamics of Antarctica with insights on Victoria Land. *Remote Sensing* **10**, 1608. doi: 10.3390/rs10101608

Zhang Q and 6 others (2020) A refined metric for multi-GNSS constellation availability assessment in polar regions. *Advances in Space Research* **66**, 655–670. doi: 10.1016/J.ASR.2020.04.033

Zumberge JF, Heflin MB, Jefferson DC, Watkins MM and Webb FH (1997) Precise point positioning for the efficient and robust analysis of GPS data from large networks. *Journal of Geophysical Research: Solid Earth* **102**, 5005–5017. doi: 10.1029/96JB03860

https://doi.org/10.1017/jog.2023.101 Published online by Cambridge University Press